A brief on Climatology of Kenya

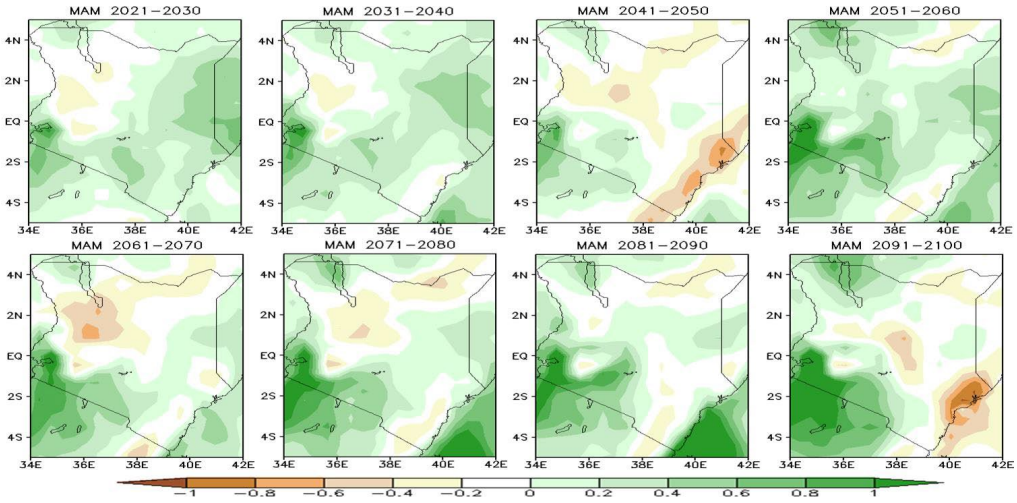

April 2021

By Kenya Meteorological Department

Annex to the GCF funding proposal titled "Enhancing community resilience and water security in the Upper Athi River Catchment Area, Kenya"

Table of Contents

Table of Figures

List of Acronyms and Abbreviations

ENSO El Niño–Southern Oscillation

EALLJ East Africa Low Level Jet

ETCCDI Expert Team on Climate Change Detection and Indices

GCMs Global Climate Models

ITCZ Inter-Tropical Convergence Zone

JJA June July August

KM Kilometers

MAM March April May

NE Northeast

OND October November December

PRCPTOT Annual total PRCP in wet days (RR >=1 mm)

R99p Annual total PRCP when RR > 99thpercentile

RACMO2 Regional Atmospheric Climate Model

RCMs Regional Climate Models

RCPs Representative Concentration Pathways

RMSE Root Mean Square Error

SST Sea Surface Temperatures

TMAXmean Annual mean maximum temperature

TMINmean Annual mean minimum temperature

TNx Monthly maximum value of daily minimum temp

TRMM Tropical Rainfall Measuring Mission

TXx Monthly maximum value of daily maximum temp

1.0 Introduction

Kenya experiences bimodal rainfall regime, which is locally referred to as 'long rains' season coming in March-May (MAM) and the 'short rains' being reported in October-December (OND) with high amounts mostly reported during the long rain season. These rainy seasons coincide with periods of the year when the ITCZ is overhead at the equator. The intervening periods are relatively dry. However, there are rainfall-enhancing mechanisms in the region, which contribute to substantial rains over the western and coastal parts of East Africa in July-August (JJA). These mechanisms include the warm and moist Congo air mass, and the East Africa low-level jet (EALLJ) respectively

The country is generally characterized by warm temperature throughout the year ranging between 19° to 30° C. January and February are the warmest months, while June and July are the coldest months.

2.0 Rainfall and Temperature Pattern, Variability and Trend

2.1 Spatial-Temporal Rainfall Pattern and Variability

Figures 2.1, 2.2 and 2.3 show the annual and seasonal spatial rainfall pattern over Kenya for the three datasets. From the figures, the western region bordering Lake Victoria, central highland of Rift Valley and part of coastal part receive the highest rainfall, with an annual mean ranging from 1000 to 2200 mm while, northern and eastern part receive lesser rainfall with an average of below 800 mm and they are mainly Arid and semi-arid (Table 2.1). The gridded dataset (GPCC and CRU) captured well the spatial rainfall pattern for both annual and seasonal mean, although it underestimates in areas that receive enhanced rainfall (2.1, 2.2 and 2.3).

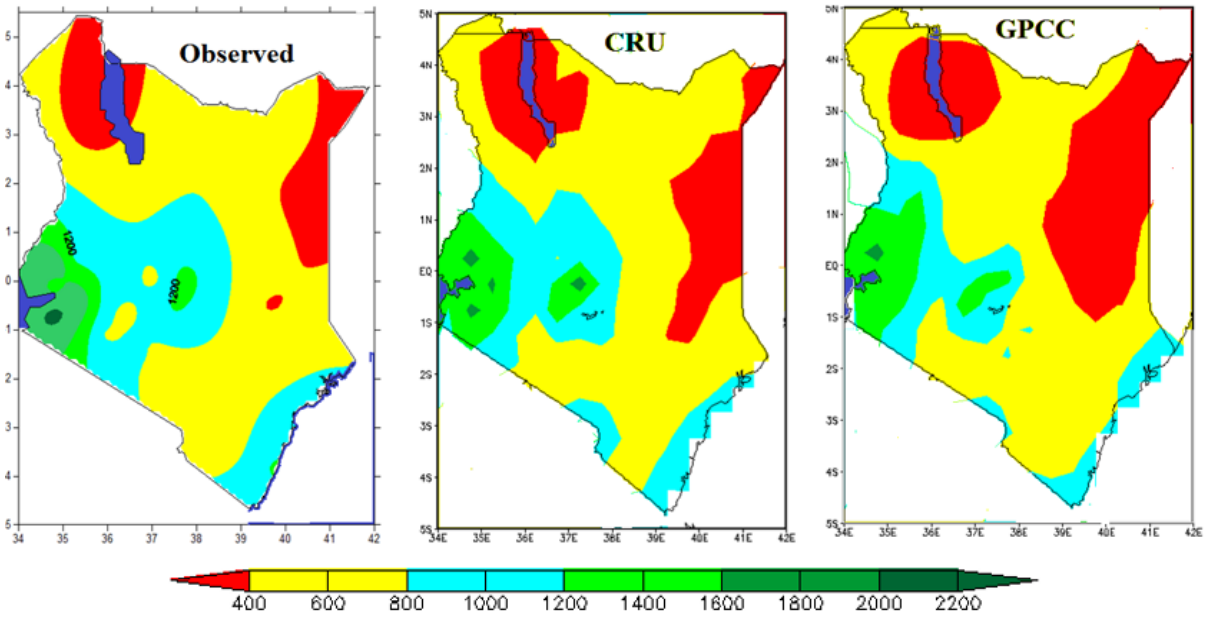

Figure 1 Climatology of annual rainfall over Kenya for station obseved, CRU and GPCC (1960- 2014)

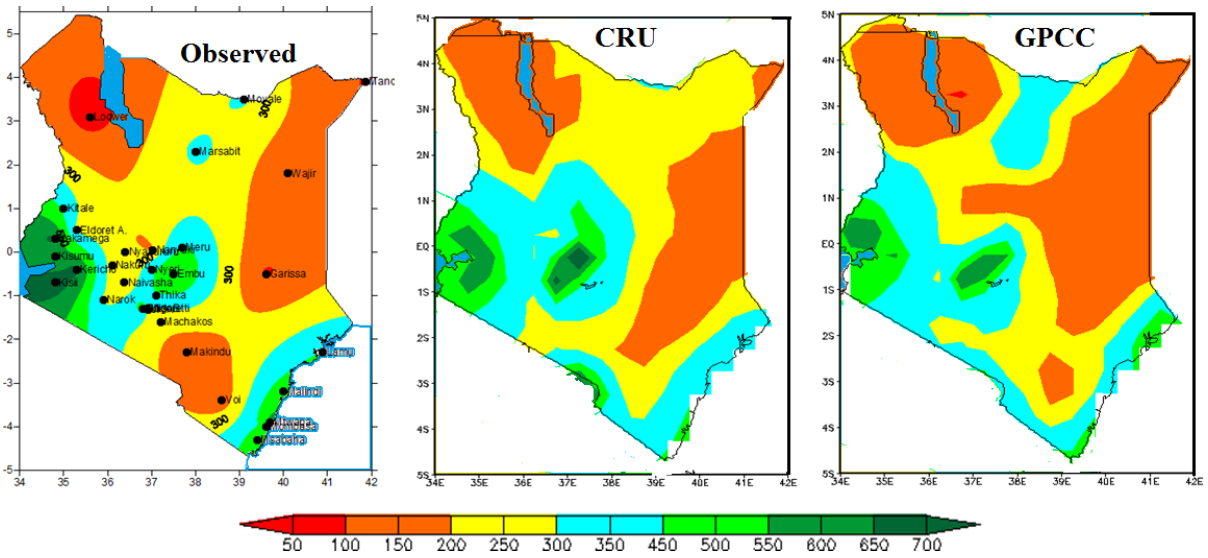

Figure 2 Climatology of MAM rainfall season over Kenya for station observed, CRU and GPCC (1960-2014)

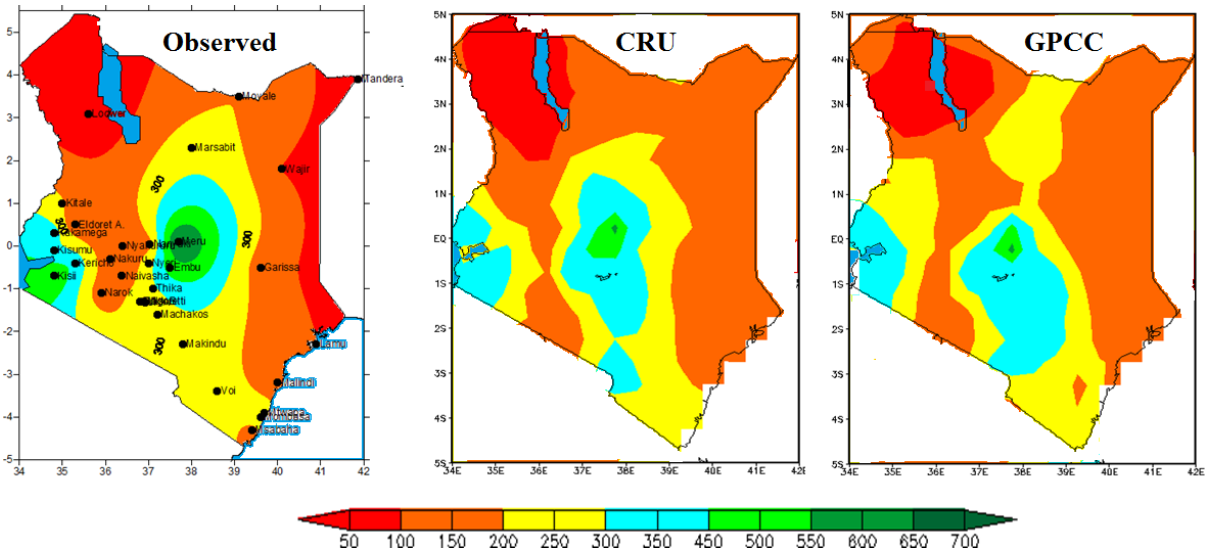

Figure 3 Climatology of OND rainfall season over Kenya for station observed, CRU and GPCC (1960-2014)

It is clear that Kenyan rainfall is Bimodal as captured by all the dataset (figure 4.5). It shows two rainfall seasons; March-May whose peak is in April which is long rain season while the short rain is from October to December with the peak in November. Figure 2.4 also shows that GPCC and CRU underestimate rainfall over Kenya as compared to the observed station data.

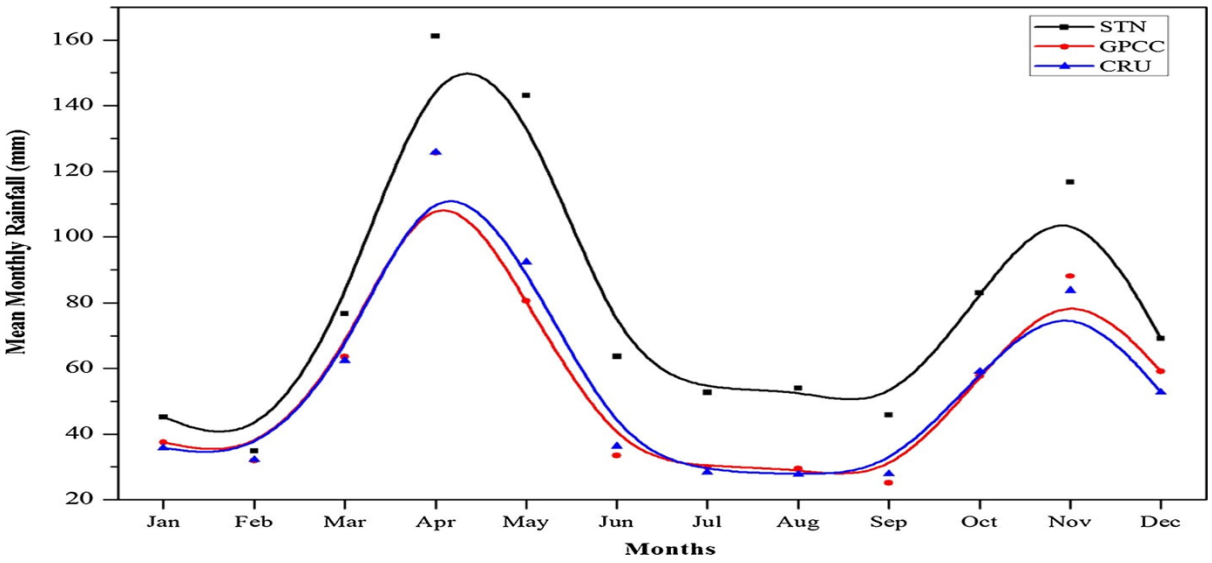

Figure 4 Annual rainfall cycle over Kenya form the Observed station data, GPCC and CRU datasets

Temporal variability of rainfall in Kenya is very high. The gridded data (GPCC and CRU) captured well the temporal variability of both seasons as shown in figure 2.5. It is also clear that the two gridded datasets underestimate the rainfall over Kenya, especially the MAM season. Generally, GPCC and CRU dataset to reproduce the spatial-temporal rainfall pattern over Kenya.

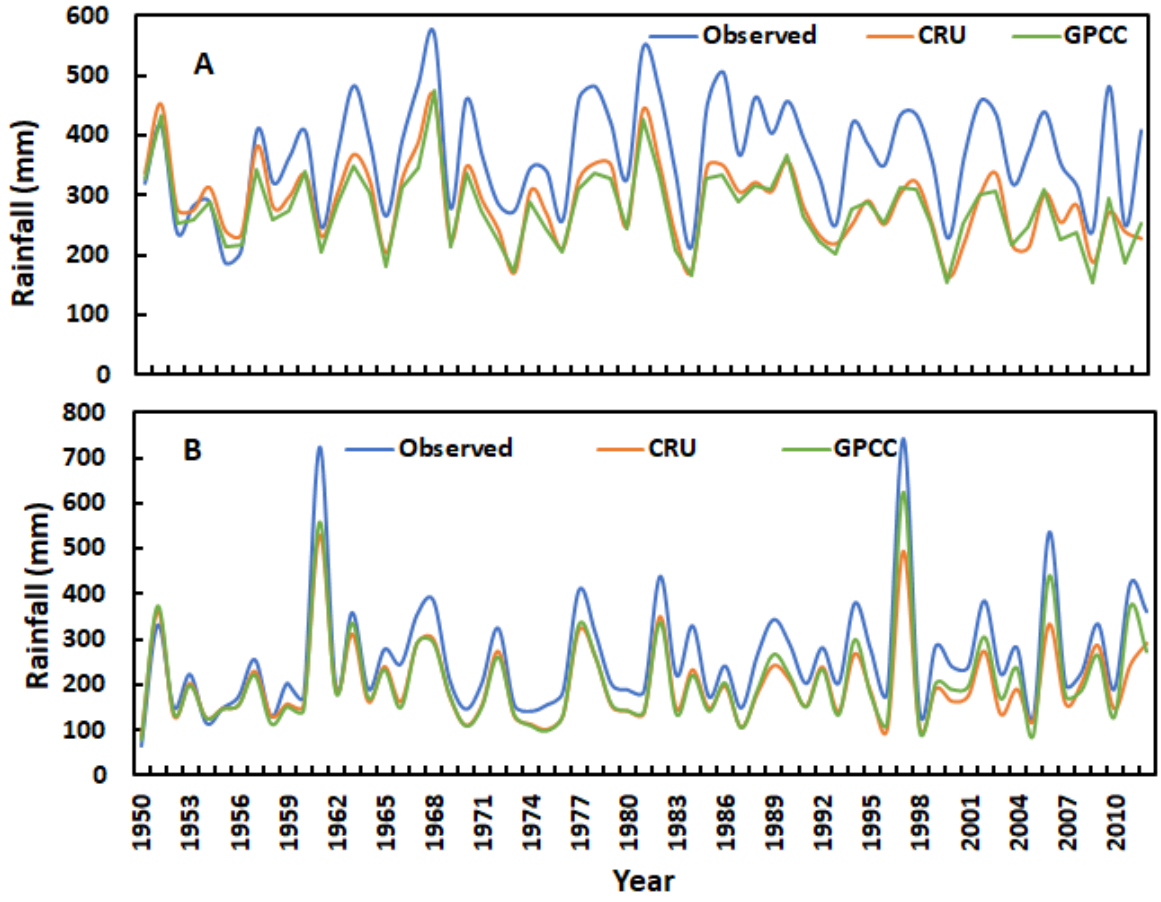

Figure 5 Time series of seasonal rainfall (a) MAM season (b) OND season for the observed, CRU and GPCC datasets over Kenya

The contribution of the two main rainfall seasons (MAM and OND) to the annual rainfall was analyzed. The results are shown in Table 4.2 whereby MAM contribute between 30 to 50% of the total annual rainfall. with the lowest percentage in Nyahururu station which MAM contribute 27% of the total annual rainfall and the highest in Mandera at 51.8% of the total annual rainfall. On the other hand, OND season contribution ranges from as low as 16% in Lamu to as high as 53.6% in Makindu. It was noted that for central, northern, western and coastal regions, MAM forms the main rainfall season while Lower Eastern region (Voi, Makindu, Meru, Garissa) much of its annual rainfall is from the short rain season (OND). The two seasons contributed less than 50% of the annual rainfall for Eldoret and Nyahururu station, while for Machakos the two seasons contribute equally to the total annual rainfall in that area. The third season (JJA) plays a great role over the western part, where the two seasons contribute less than 60% of the total annual rainfall. Although the two seasons (MAM and OND) have been recognized as the main rainfall season, JJA season cannot be ignored due to its contribution in western part of Kenya. It is important therefore that the changes of JJA season also be analyzed and its future projections are in cooperated in climate change assessment.

Table 1 Annual and seasonal (MAM and OND) means (mm) for 33 stations and their percentage (%) contribution to the Annual rainfall

No.	Station Name	MAM Mean	OND Mean	Annual Mean	% Contribution of MAM to annual rainfall	% Contribution of OND to annual rainfall	Total % Contribution of MAM and OND to annual rainfall
1	Lodwar	99.7	50.3	215.3	46.3	23.3	69.6
2	Kericho	681.8	431.0	2023.1	33.7	21.4	55.1
3	Machakos	287.4	291.5	695.3	41.3	41.9	83.3
4	Kisumu	535.5	355.1	1388.6	38.6	25.6	64.1
5	Kisii	696.7	529.9	2105.0	33.1	25.2	58.3
6	Voi	192.5	280.6	566.3	34.0	49.6	83.6
7	Makindu	188.1	310.7	579.4	32.5	53.6	86.1
8	Marsabit	368.3	302.9	774.3	47.6	39.1	86.7
9	Narok	339.2	182.5	780.1	43.5	23.4	66.9
10	Kakamega	676.8	405.2	1970.3	34.3	20.6	54.9
11	Thika	441.9	332.7	935.19	47.3	35.6	82.8
12	Mtwapa	583.2	291.2	1291.1	45.2	22.6	67.7
13	Mombasa	454.9	285.4	1061.5	42.9	26.9	69.7
14	Embu	579.4	495.5	1269.1	45.7	39.0	84.7
15	Nyeri	418.2	303.4	938.7	44.5	32.3	76.9
16	Dagoretti	488.1	315.3	1034.2	47.2	30.5	77.7
17	Meru	459.6	686.1	1328.6	34.6	51.6	86.2
18	Kitale	441.5	261.7	1274.1	34.7	20.5	55.2

19	Nakuru	319.4	194.6	946.3	33.8	20.6	54.3
20	Nyahururu	274.0	190.5	998.1	27.5	19.1	46.5
21	Wajir	159.0	147.9	331.8	47.9	44.6	92.5
22	Moyale	360.1	247.7	707.1	50.9	35.0	86.0
23	Malindi	507.0	190.8	1075.4	47.1	17.7	64.9
24	Eldoret A.	328.5	162.0	1063.3	30.9	15.2	46.1
25	Mandera	143.6	120.0	277.2	51.8	43.3	95.1
26	Garissa	138.5	191.3	374.2	37.0	51.1	88.1
27	Lamu	455.7	152.6	954.8	47.7	16.0	63.7
28	Msabaha	513.5	237.2	1160.4	44.2	20.4	64.7
29	M.A.B	411.4	274.2	884.4	46.5	31.0	77.5
30	Wilson	426.7	285.4	923.2	46.2	30.9	77.1
31	JKIA	314.5	259.7	737.6	42.6	35.2	77.8
32	Nanyuki	242.6	208.1	690.3	35.1	30.2	65.3
33	Naivasha	250.6	179.6	668.9	37.5	26.8	64.3

2.2 Spatial-Temporal Temperature Pattern

The annual cycle of maximum and minimum temperature over Kenya based on CRU datasets and station observed data is presented in figure 2.6. It shows that the lowest temperature is reported during June- August (JJA) season, while December-February (DJF) is the hottest season, it extends to earlier March. The cold season is due to the push of cold and less moist low-level airmass northwards by the Mascarene high during the southern hemisphere winter (Manatsa et al., 2014). CRU dataset captures the annual cycle but it overestimate both minimum and maximum temperature.

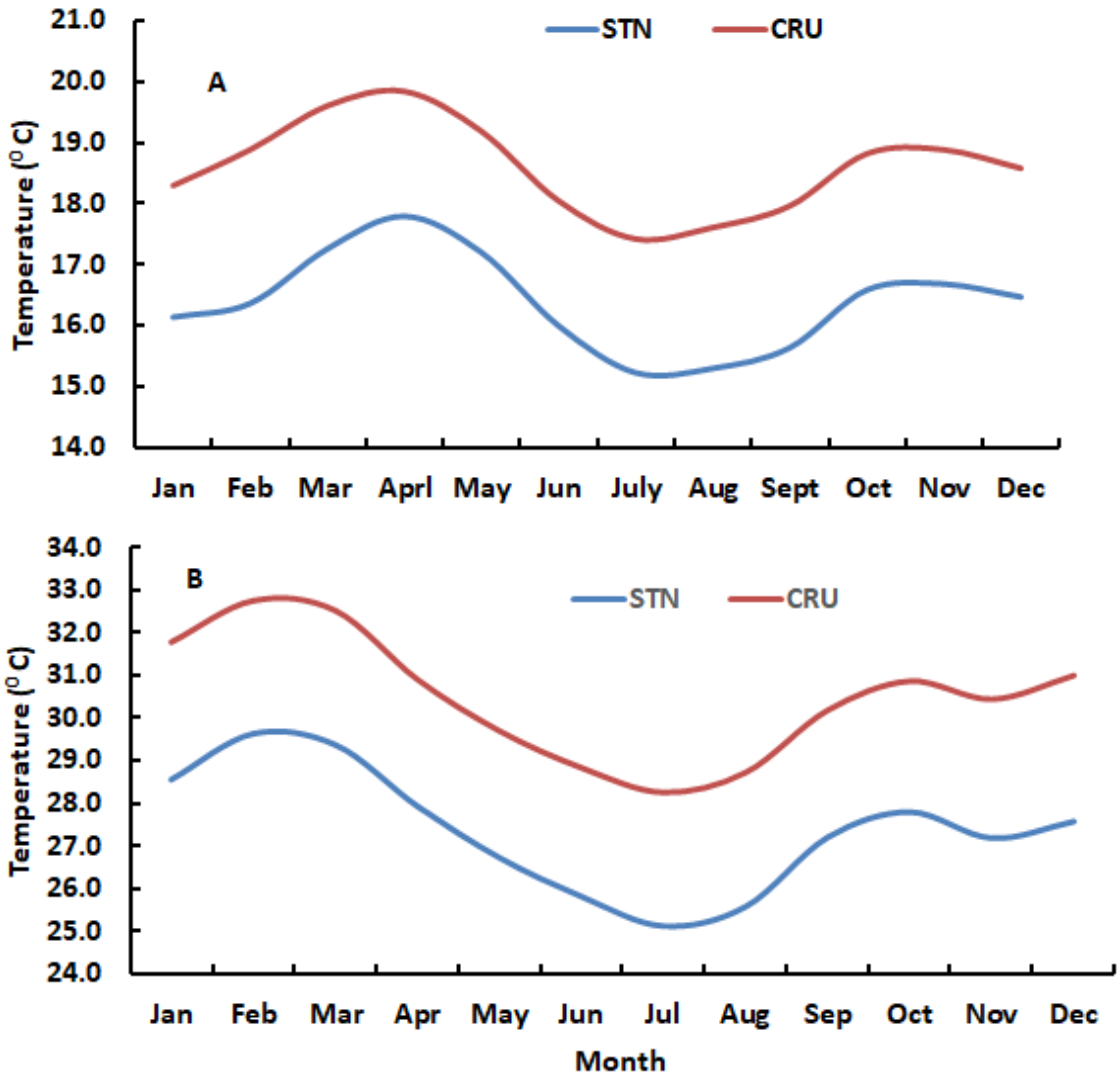

Figure 6 Annual temperature cycle over Kenya for (a) Minimum (b) Maximum, where the red line show station observed data and blue for CRU data

The Climatology of the temperature based on the observed and CRU dataset is presented in Figure 4.9. It shows that eastern and northern parts of Kenya record high temperatures while the western and central parts recoding lowest temperature. CRU was also able to capture the spatial temperature variability over Kenya.

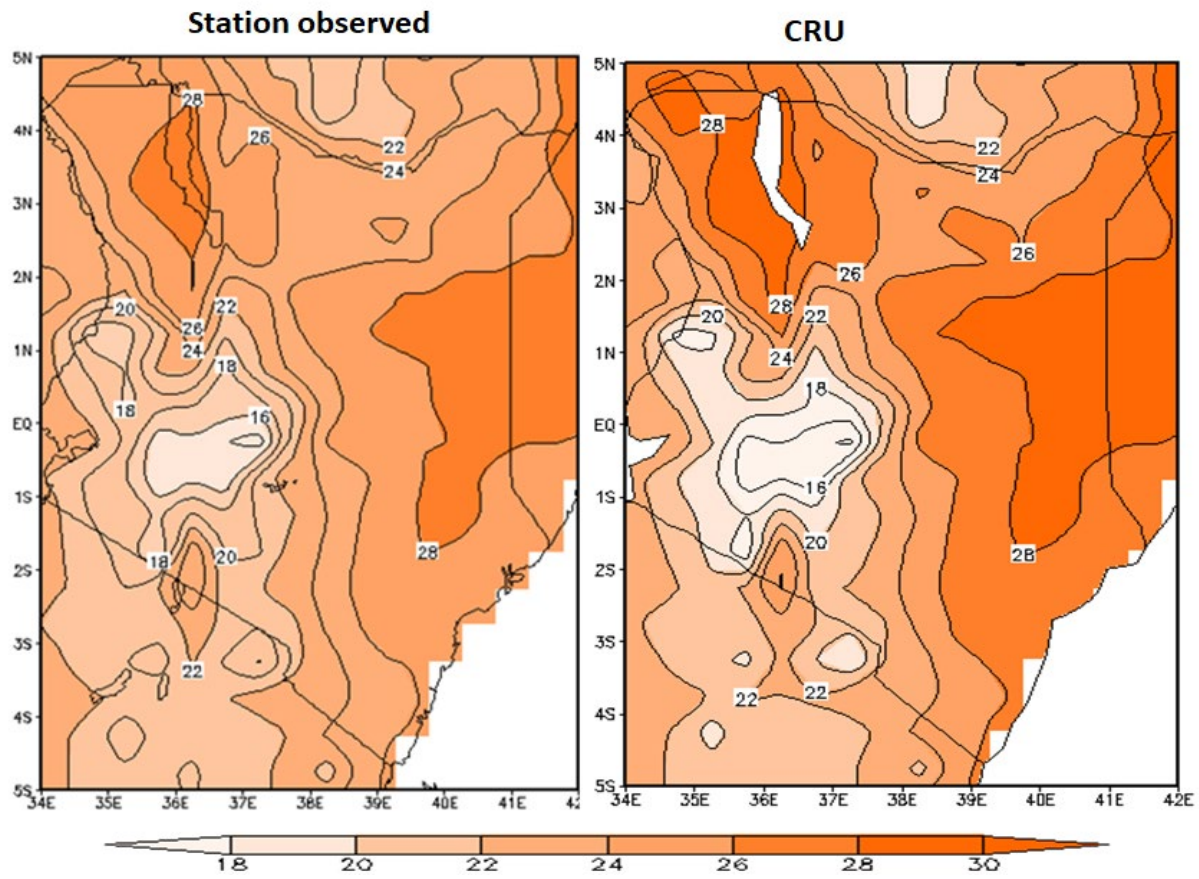

Figure 7 Climatology of mean temperature over Kenya based on station observed and CRU datasets for a period (1980-2014).

The mean maximum temperature (Tmx), minimum temperature (Tmin) and temperature range (R) which is the difference between the maximum and minimum temperature for the station are shown in figure 2.8, The Temperature range between 35.5 to 23.3 ^{o}C, while the Tmin is 24 to 9.6 ^{o}C. The coastal station (Lamu, Mombasa, Malindi, and Mtwapa) had the lowest R of between 6 and 8 ^{o}C, while Narok station had the highest temperature range of 15.4 ^{o}C. Figure 4.11 shows the monthly climatology of R over Kenya. In the month of February to March show some higher values of temperature range are observed over most of part of the country. Low values are observed during the month of May to August. The coastal region shows a low-temperature range for all the months of the year. The low-temperature range at the coast may be due to low altitude and humid atmosphere as a result of the moisture from the adjacent Indian Ocean. The moist air in the coastal region has higher heat capacity than dry air, limiting the rate of atmospheric warming and cooling as compared to dry inland air. The humid air is dynamically associated with low-level cloud cover which inhibits incoming solar radiation.

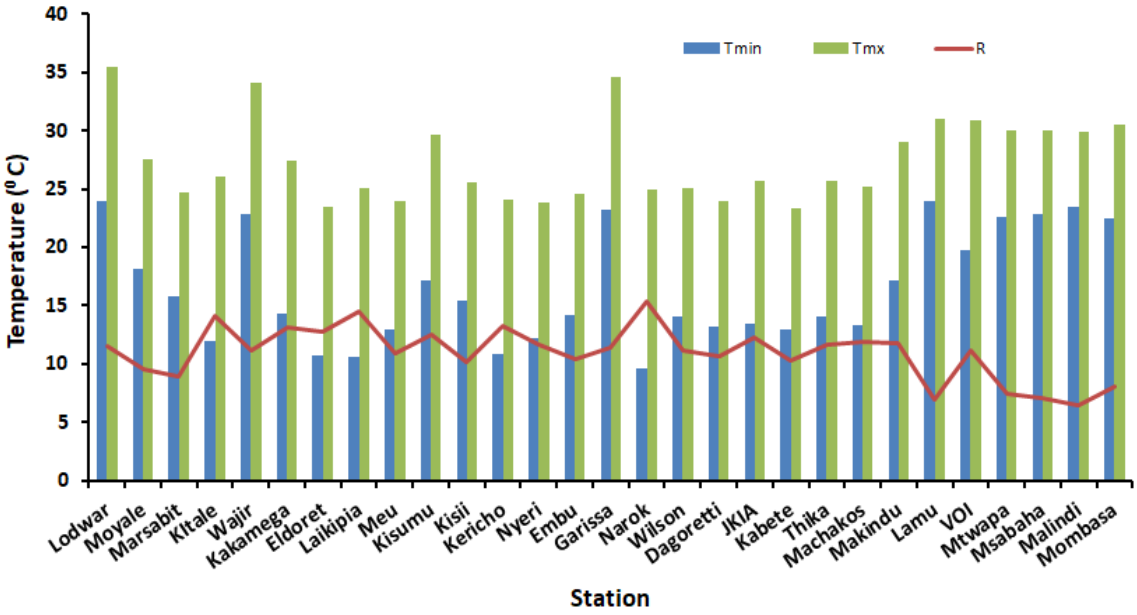

Figure 8 Mean maximum temperature (Tmx), minimum temperature (Tmin) and temperature range (R) for the various stations over Kenya

It was also noted that during the rainy season MAM and OND, the temperature range was low as compared to DJF which is the dry season. An analysis on temperature range over East Africa, is attributed the low-temperature range during the rainy season to the cloud cover, it is noted that Cloud cover has a significant negative correlation to temperature range over East Africa. This is also the case as seen in figure 2.9 where January and February which are dry months have high-temperature range. Therefore, January and February are the months that observe the highest temperature range while June -July is low-temperature range months.

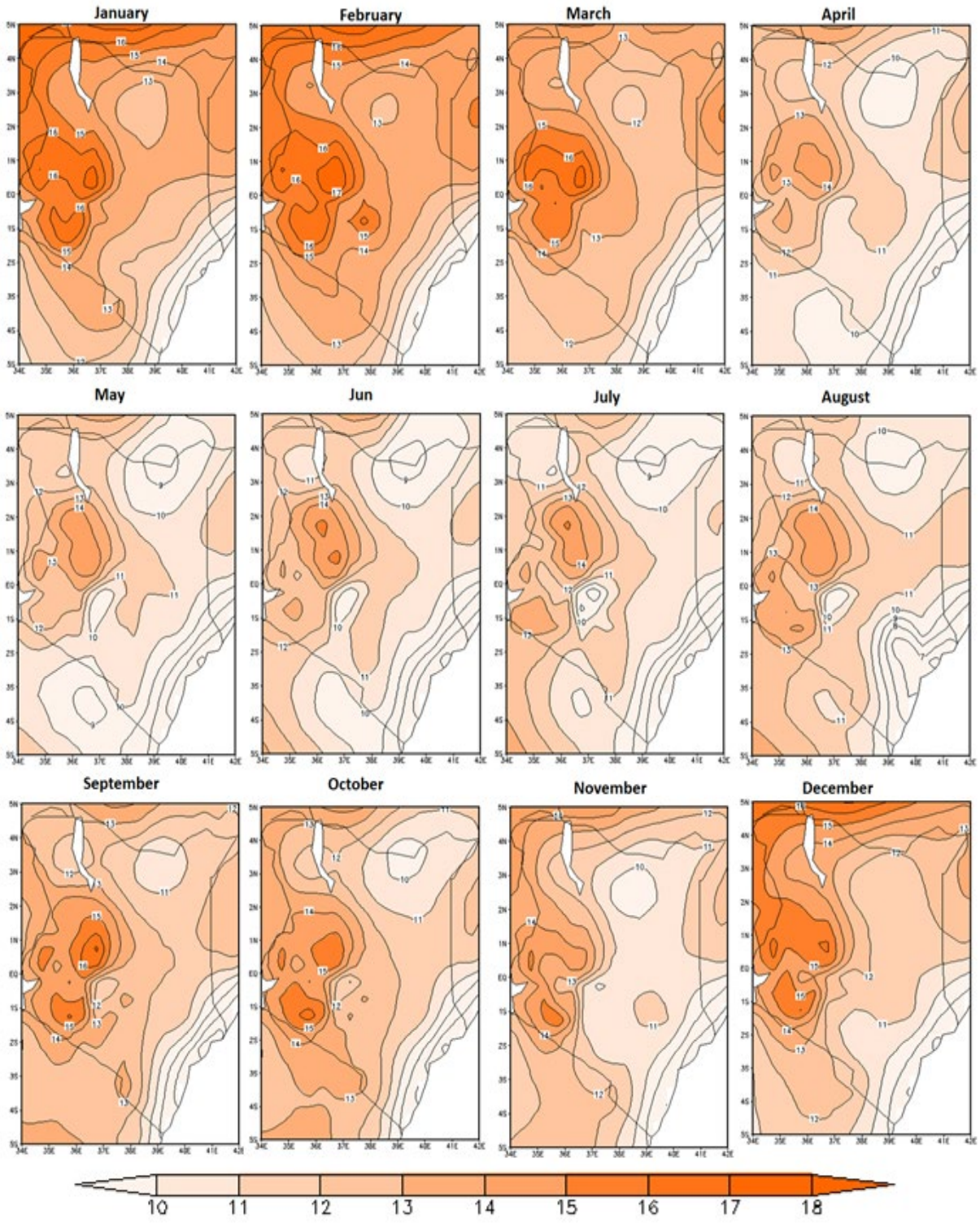

Figure 9 Temperature range Monthly climatology (°C) over Kenya for January – December) based on the CRU datasets for the period 1970 – 2015.

2.3 Rainfall Trend Analysis

Figures. 2.10 to 2.13 shows decadal variability of rainfall for MAM and OND seasons, based on CRU and GPCC datasets. The results show that in the last two decades higher negative anomaly than the earlier decade (Figure 2.10 and 2.11), in the recent past MAM season has been experienced a reduction in rainfall, relative to the long-term mean of 1981 to 2010. The decade of 1910's and that of 1960's were the wettest MAMs. For the OND season, it has shown a relative increase in rainfall over the last recent past (2001-2010) (Figure 2.12 – 2.13). 1960's recorded the highest rainfall for both MAM and OND seasons as compared to the other decades, this was due to the positive IOD and a very strong Turkana

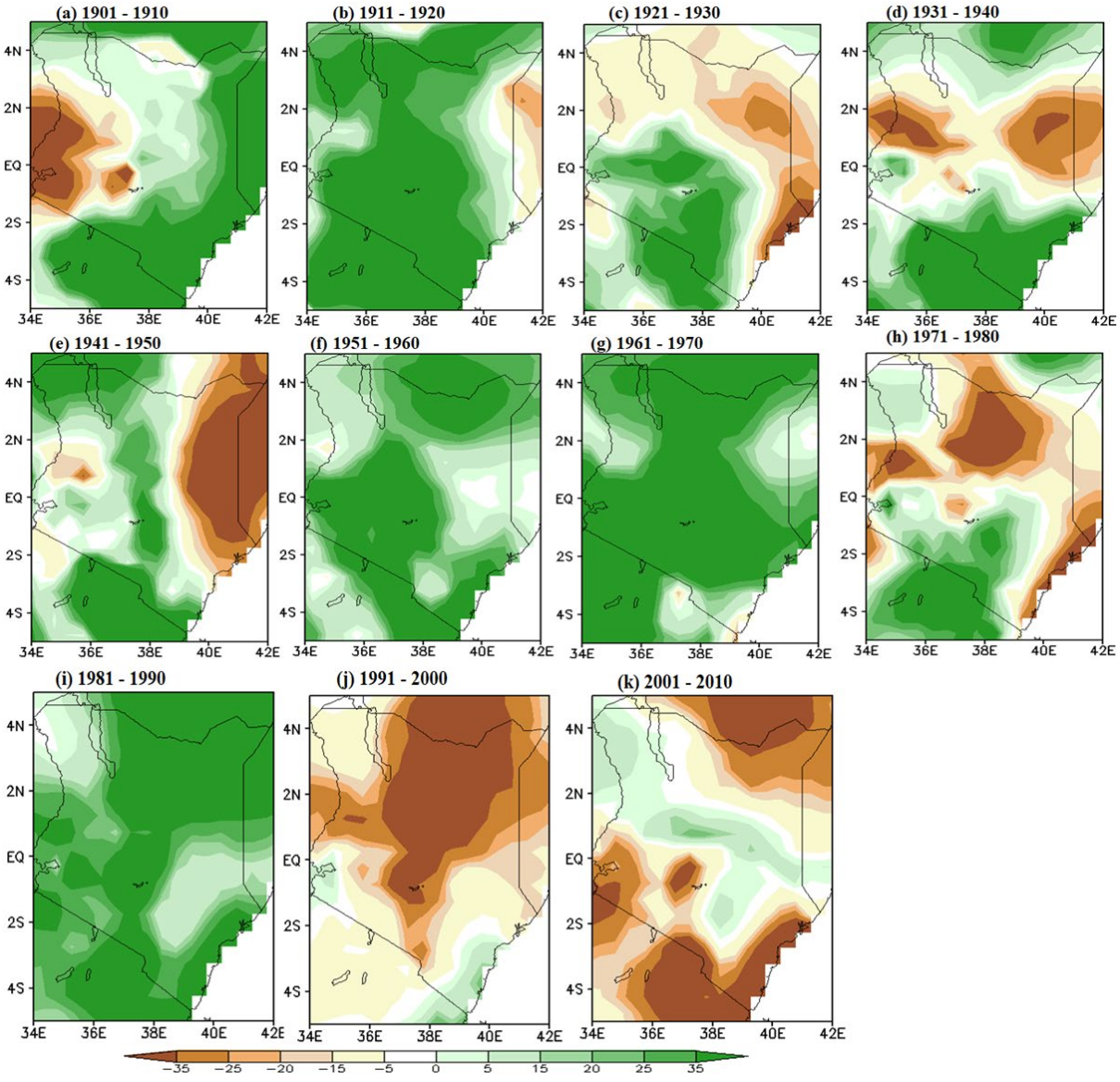

Figure 10 Decadal change in March-May rainfall anomaly from 1901 to 2010 relative to the base period of 1981 – 2010 over Kenya based on CRU datasets

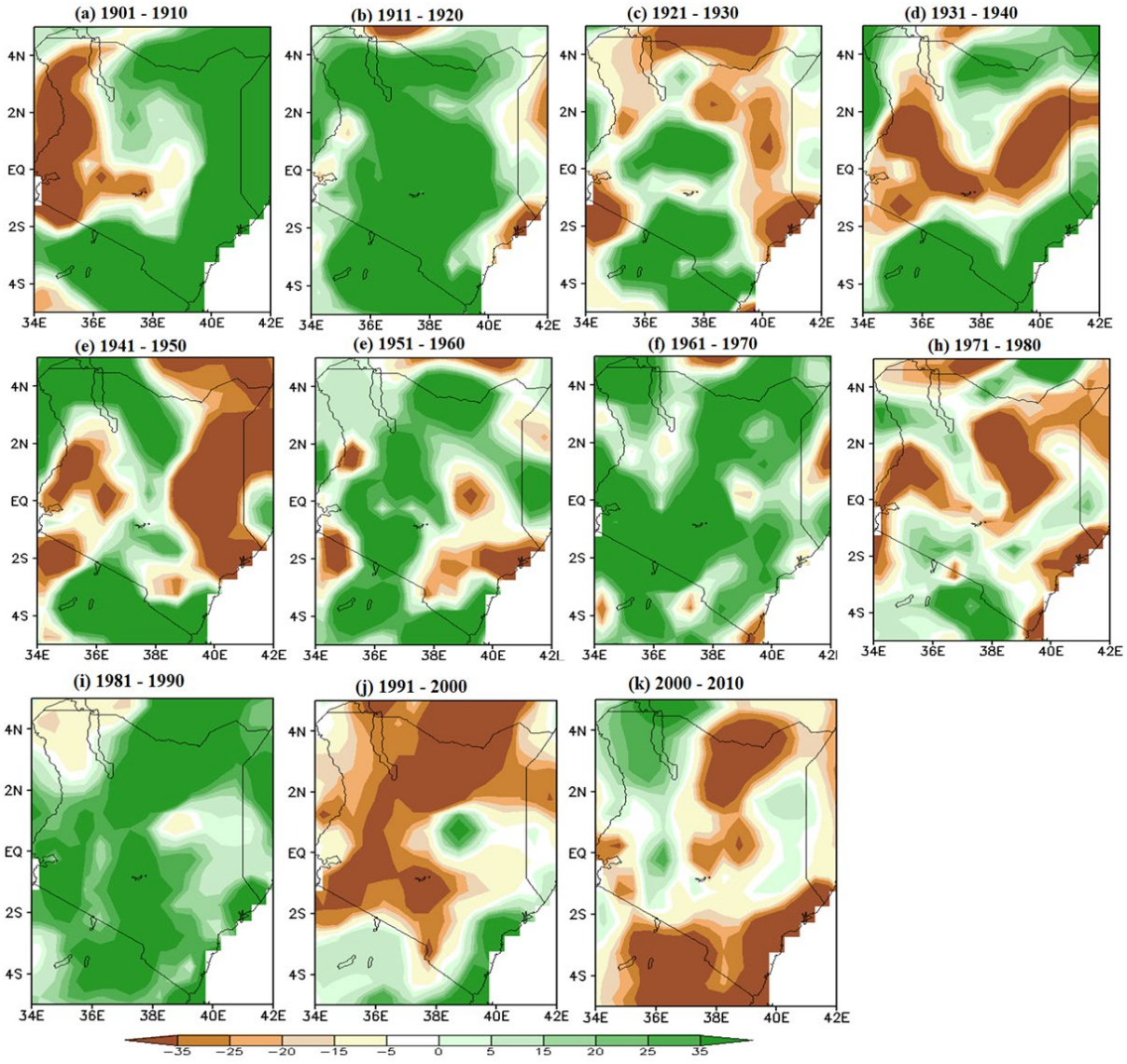

Figure 11 Decadal change in March-May rainfall anomaly from 1901 to 2010 relative to the base period of 1981 – 2010 over Kenya based on GPCC datasets

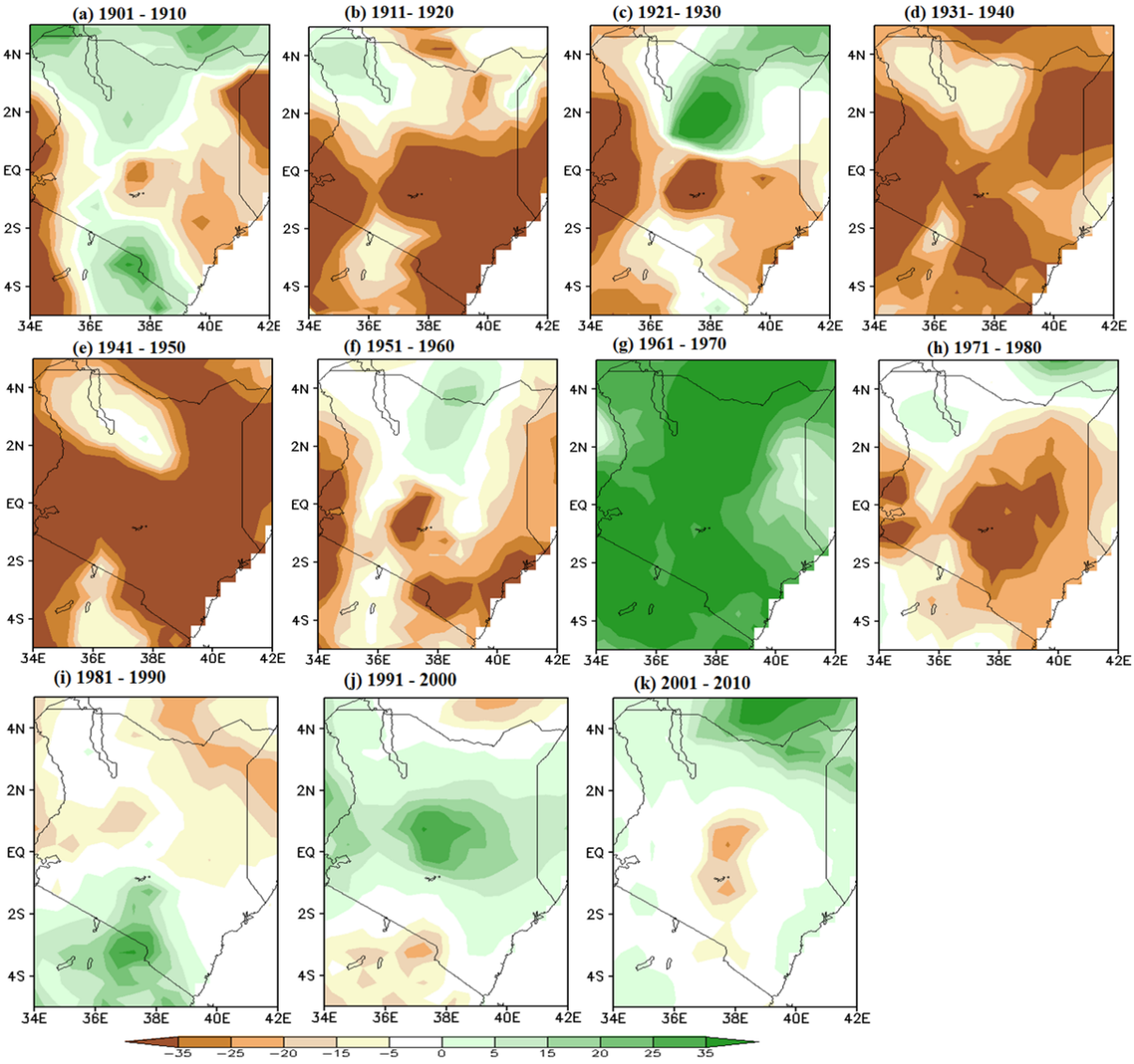

Figure 12 Decadal change in October-December rainfall anomaly from 1901 to 2010 relative to the base period of 1981 – 2010 over Kenya based on CRU datasets

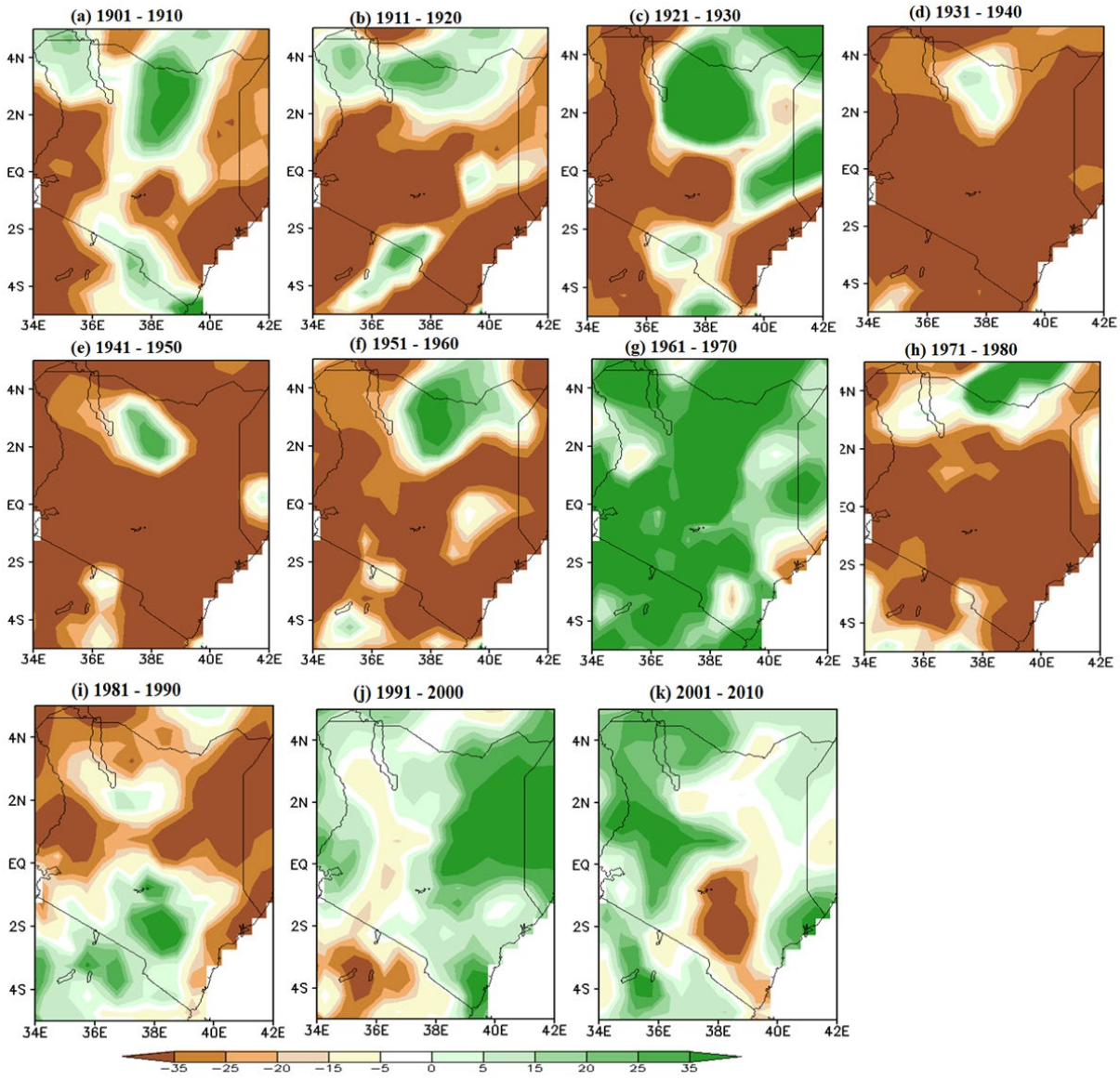

Figure 13 Decadal change in October-December rainfall anomaly from 1901 to 2010 relative to the base period of 1981 – 2010 over Kenya based on GPCC datasets

Rainfall during the MAM season exhibited a decreasing trend while that for OND exhibited an increasing trend (Table 2.2). However, the trends are statistically insignificant at 5% significance level for both seasons (OND and MAM). But some stations (Marsabit and Moyale) displayed a statistically significant decreasing trend for MAM season at 5% significant level, while Kitale and Nakuru stations had a significant increasing trend for OND season. However, Nanyuki displayed a statistically significant decreasing trend for OND season. increasing and decreasing trend which is insignificant at 5% significant level were noted for the different station in the annual mean rainfall, with exception of Moyale which had significantly decreasing trend at 3.52 mm/year (Table 2.2). Figure 2.14 shows the spatial MK test statistic where countrywide decreasing rains during the MAM season and increasing in OND is noted. Although there is a decreasing (increasing) in rainfall over areas some station during OND (MAM). For example, during MAM season some part of Lake Victoria area indicate an increasing

trend even though it is statistically insignificant. The same case applies for the OND season (figure 2.14). Therefore, it is important not to generalize the increase and decrease in rainfall. Several studies have indicated that in East Africa rainfall is declining during MAM and increasing in OND (Liebmann et al., 2014; Yang et al., 2014). The increase has been attributed to the warming of the western Indian Ocean (Liebmann et al., 2014). While Yang et al. (2014) attributed the declining rainfall during MAM to natural decadal variability and not anthropogenically related. The results from the two studies and several others cannot be used for adaptation strategies since the increase (decrease) is different from one climatological region to another within Kenya (Figure 2.14).

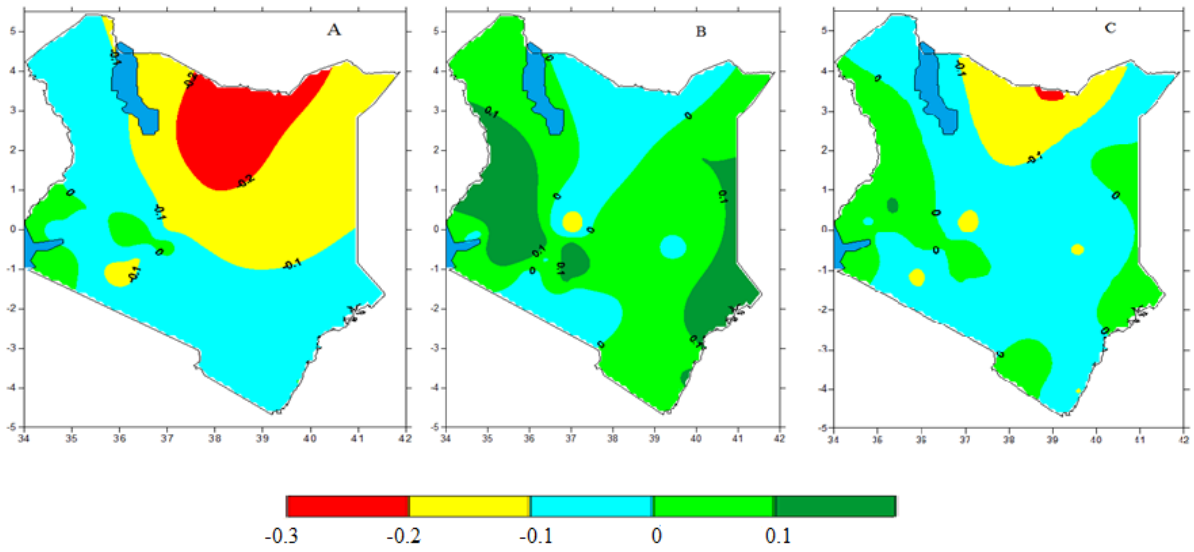

Figure 14 Spatial distribution of Mann-Kendall (MK) at 5% level of significance statistics for (a) MAM, (b) OND and (c) Annual

Table 2 Mann-Kendall (MK) statistics, Sen's slope and P-value for MAM, OND and Annual for different station (highlighted in red show statistically significant at 5% level)

No	Station Name	MAM			OND			ANNUAL		
		MK	Sen's slope	p-value	MK	Sen's slope	p-value	MK	Sen's slope	p-value
1	Lodwer	-0.046	-0.226	0.598	0.066	0.106	0.451	0.01	0.085	0.92
2	Kericho	-0.109	-2.168	0.336	0.279	0.012	6.01	-0.072	-2.44	0.532
3	Machakos	-0.060	-0.718	0.520	-0.031	-0.199	0.740	-0.070	-1.383	0.450
4	Kisumu	-0.086	-1.12	0.363	-0.024	-0.27	0.800	0.010	0.138	0.917
5	Kisii	0.102	1.7	0.300	0.050	0.671	0.616	0.063	1.89	0.525
6	Voi	-0.010	-0.065	0.915	0.097	1.067	0.262	0.044	0.743	0.618

7	Makindu	-0.067	-0.375	0.441	-0.033	-0.304	0.704	-0.030	-0.574	0.731
8	Marsabit	-0.283	-2.407	0.020	-0.032	0.433	0.717	-0.138	-3.723	0.111
9	Narok	-0.137	-1.46	0.115	-0.021	-0.171	0.812	-0.123	-2.035	0.155
10	Kakamega	0.016	0.254	0.867	0.119	1.551	0.201	-0.013	-0.392	0.896
11	Thika	-0.031	-0.544	0.740	0.168	2.11	0.069	0.073	1.726	0.433
12	Mtwapa	0.010	0.289	0.917	0.153	1.847	0.104	-0.009	-0.197	0.929
13	Mombasa	-0.078	-1.656	0.400	-0.016	-0.079	0.871	-0.131	-3.395	0.155
14	Embu	-0.069	-1.49	0.559	0.057	1.202	0.631	-0.027	-1.28	0.825
15	Nyeri	0.044	0.838	0.676	0.162	2.45	0.120	0.073	2.45	0.490
16	Dagoretti	-0.036	-0.544	0.697	0.099	1.1	0.277	-0.005	-0.134	0.957
17	Meru	-0.162	-3.04	0.111	0.067	1.8	0.515	-0.014	-0.444	0.898
18	Kitale	-0.005	-0.075	0.977	0.301	5.062	0.012	0.094	4.733	0.444
19	Nakuru	0.053	0.636	0.601	0.286	2.04	0.004	0.063	1.24	0.531
20	Nyahururu	0.050	0.564	0.608	0.039	0.366	0.687	0.011	0.341	0.918
21	Wajir	-0.120	-0.706	0.167	0.101	0.66	0.243	0.026	0.303	0.767
22	Moyale	-0.245	-2.77	0.005	-0.082	-0.86	0.343	-0.228	-3.52	0.008
23	Malindi	-0.050	-0.923	0.608	0.055	0.709	0.570	-0.083	-1.995	0.390
24	Eldoret A.	0.000	-0.022	0.991	0.232	3.52	0.033	0.117	3.86	0.288
25	Mandera	-0.173	-1.088	0.061	0.031	0.207	0.745	-0.029	-0.437	0.761
26	Garissa	-0.113	-1.093	0.230	-0.022	-0.177	0.823	-0.111	-1.45	0.239
27	Lamu	-0.045	-0.854	0.610	0.327	2.711	0.000	0.117	2.71	0.178
28	Msabaha	-0.008	-0.155	0.938	0.082	1.00	0.377	-0.029	-0.673	0.761
29	M.A.B	-0.018	-0.291	0.865	0.142	1.49	0.168	0.047	1.57	0.651
30	Wilson	-0.100	-1.895	0.280	0.169	1.712	0.067	-0.035	-0.815	0.708
31	JKIA	-0.041	-0.508	0.663	0.041	0.369	0.663	-0.058	-1.363	0.537
32	Nanyuki	-0.134	-1.236	0.147	-0.206	-1.024	0.025	-0.166	-2.635	0.073
33	Naivasha	-0.109	-1.00	0.259	-0.021	-0.172	0.831	-0.050	-0.77	0.608

Figure2.15 represents the Mann-Kendall test for abrupt changes for the annual mean rainfall. There was a general decrease in rainfall from mid-1960s to late 2000s. The forward and backward sequential statistics intersected around twice in 1952 and about five times in 1980, which form periods of a trend change. However, there was no observed abrupt change throughout the study period. The changes in rainfall are insignificant throughout the study period with an exception of 1962 when a significant positive change was recorded

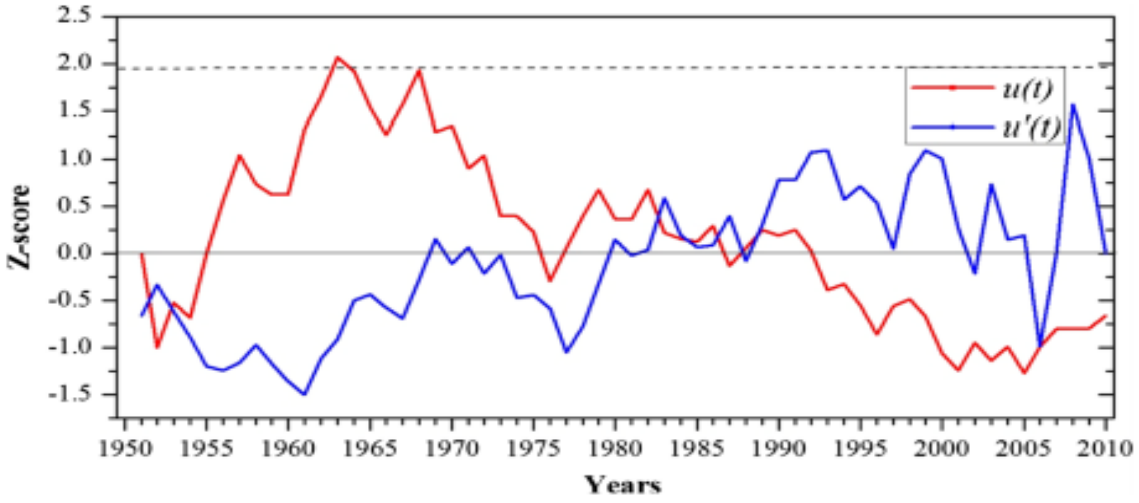

Figure 15 Abrupt change in annual rainfall over Kenya where the red is for forward sequential blue is for backward sequential statistic and the dashed lines represent the confidence limits at 5%.

2.4 Temperature Trend Analysis

The Mann-Kendall test statistics results for the seasonal change in minimum temperature (Tmin) and maximum Temperature (Tmax) are shown in Table 2.3 and 2.4 respectively. They show a positive trend in both Tmax and Tmin for most stations analyzed. The increasing trend of Tmin is statistically significant at $p < 0.05$ in most of the stations, while that of Tmax, the station exhibits an increasing trend but for most of them, it is statistically insignificant. However, about 10% of the stations showed a decreasing trend which is not statistically significant at $p < 0.05$.

During DJF season, Tmin shows an increasing trend, which is statistically significant at $p<0.05$ in 70% of all the stations. However, 5% of the stations have a decreasing trend, which is not statistically significant. Tmax increasing trend was realized but it statistically insignificant. During MAM season the warming was noted in most of the station, which was statistically significant for Tmin, only 31% of the stations showed an increasing trend which is statistically insignificant. On the other hand, the Tmax about 50% of the station showed a statistically significant increasing trend.

During the northern summer season, which is noted as the coldest months in Kenya (JJA), it showed a warming trend in Tmin for more than 80% of the stations. Similar results were noted in Tmax. OND season showed an increasing trend in Tmin and Tmax, which is significant at $p < 0.05$ level for most of the stations but for fewer station on Tmax. It was noted Tmin had a statistically significant increasing trend, for all the four stations that are based in Nairobi namely; Dagorreti, Wilson, JKIA, and Kabete. The increase in Tmax for these Nairobi stations were not statistically significant. The Mann-Kendall test confirms that there is an increasing trend in annual Tmax and Tmin Over Kenya, which is statistically significant at $p < 0.05$ level. However, Narok and Garissa stations showed a negative trend which is not statistically significant for Tmin, while Kakamega exhibited the same result for Tmax. The slope (S) for the annual Tmax and Tmin ranges from 0.048 ^{o}C/year to 0.012 ^{o}C/year. This trend corresponds to an increase of 0.3 ^{o}C to 1.44 ^{o}C.

It is evident that most of the station had an increasing trend for both Tmin and Tmax and the increase was higher during the cold season as compared the dry season. This confirms the overall warming of the country. Finding from studies conducted by Makokha and Shisanya, (2010), Omondi et al., 2014, Ngaina and Mutai, (2013), Opiyo at al. (2014), obtained similar findings that there is a significant increasing trend in Tmin than that of Tmax. The increase can be attributed to the increase in greenhouse gases emissions, hence warming.

Overall the increase can be attributed to the ongoing global warming, coupled with other mesoscale factors, such as land use and land cover changes (Seneviratne et al., 2012).

Table 3 Mann-Kendall trend test results for Tmin (Z and p-value) and the slope S.

Station Name	DJF			MAM			JJA			SON		
	Z	P-value	S (°C/Y)	Z	P-value	S (°C/Y)	Z	P-value	S (°C/Y)	Z	P-value	S (°C/Y)
Lodwar	-0.10	0.453	-0.01	0.04	0.764	0.007	0.38	0.005	0.031	0.17	0.202	0.02
Moyale	0.197	0.081	0.014	0.43	0.000	0.022	0.49	0.000	0.031	0.54	0.000	0.031
Marsabit	0.508	0.000	0.034	0.42	0.000	0.027	0.43	0.000	0.033	0.48	0.000	0.033
Kitale	0.516	0.000	0.045	0.59	0.000	0.036	0.59	0.000	0.042	0.75	0.000	0.058
Wajir	0.099	0.383	0.007	0.231	0.044	0.02	0.38	0.001	0.022	0.43	0.000	0.023
Kakame	0.174	0.147	0.012	-0.04	0.744	-0.00	0.32	0.007	0.019	0.40	0.001	0.025
Eldoret	0.150	0.227	0.013	0.179	0.158	0.017	0.32	0.010	0.035	0.45	0.000	0.051
Laikipia	-0.01	1.0	-0.01	0.126	0.528	0.028	0.42	0.027	0.058	0.09	0.651	0.029
Meru	0.116	0.320	0.012	0.204	0.079	0.012	0.49	0.000	0.027	0.32	0.007	0.018
Kisumu	0.225	0.046	0.014	0.279	0.013	0.021	0.65	0.000	0.037	0.61	0.000	0.036
Kisii	0.410	0.000	0.023	0.375	0.002	0.021	0.50	0.000	0.026	0.44	0.000	0.023
Kericho	0.375	0.002	0.038	0.429	0.001	0.042	0.56	0.000	0.06	0.59	0.000	0.048
Nyeri	0.040	0.744	0.004	0.150	0.211	0.013	0.44	0.000	0.024	0.42	0.00	0.036
Embu	0.317	0.006	0.027	0.269	0.019	0.017	0.26	0.026	0.019	0.42	0.000	0.022
Garassa	0.328	0.005	0.021	0.334	0.004	0.024	0.22	0.061	0.017	0.28	0.016	0.017
Narok	0.408	0.000	0.052	0.361	0.002	0.05	0.49	0.000	0.058	0.56	0.000	0.08
Wilson	0.393	0.003	0.042	0.454	0.001	0.043	0.47	0.000	0.044	0.41	0.003	0.046
Dagorriti	0.459	0.000	0.033	0.611	0.000	0.035	0.54	0.000	0.036	0.65	0.000	0.042
JKIA	0.471	0.001	0.073	0.335	0.013	0.032	0.51	0.000	0.056	0.57	0.000	0.087
Kabete	0.555	0.000	0.031	0.540	0.000	0.031	0.57	0.000	0.037	0.56	0.000	0.033
Thika	0.165	0.168	0.021	0.231	0.053	0.017	0.06	0.609	0.004	0.36	0.003	0.035
Machak	0.207	0.088	0.018	0.146	0.244	0.012	0.27	0.030	0.026	0.25	0.047	0.023
Makindu	0.265	0.017	0.014	0.305	0.006	0.017	0.21	0.056	0.014	0.35	0.002	0.017
Lamu	-0.25	0.025	-0.02	0.022	0.848	0.001	0.17	0.135	0.01	-0.2	0.095	-0.01
Voi	0.521	0.000	0.027	0.497	0.000	0.024	0.43	0.000	0.025	0.48	0.000	0.028
Mtwapa	0.345	0.008	0.033	0.396	0.002	0.042	0.55	0.000	0.04	0.46	0.001	0.045
Malindi	0.340	0.003	0.017	0.564	0.000	0.036	0.41	0.000	0.025	0.60	0.000	0.03
Msabah	0.489	0.000	0.033	0.771	0.000	0.052	0.75	0.000	0.054	0.71	0.000	0.047
Mombas	0.168	0.209	0.026	0.272	0.05	0.033	0.28	0.045	0.023	0.16	0.272	0.019

Table 4 Mann-Kendall trend test results for Tmax (Z and p-value) and the slope S.

Station Name	DJF			MAM			JJA			SON		
	Z	P-value	S (°C/Y)	Z	P-value	S (°C/Y)	Z	P-value	S (°C/Y)	Z	P-value	S (°C/Y)
Lodwar	0.180	0.153	0.014	0.126	0.322	0.017	0.34	0.007	0.023	0.253	0.044	0.027

Moyale	0.293	0.010	0.036	0.235	0.045	0.035	0.24	0.048	0.028	0.359	0.002	0.028
Marsabit	0.192	0.094	0.019	0.249	0.032	0.03	0.07	0.582	0.004	0.255	0.031	0.016
Kitale	0.139	0.233	0.013	0.277	0.017	0.03	0.48	0.000	0.033	0.308	0.010	0.021
Wajir	0.287	0.012	0.026	0.326	0.006	0.039	0.44	0.000	0.045	0.371	0.001	0.04
Kakame	0.360	0.003	0.033	0.335	0.006	0.037	0.49	0.000	0.033	0.293	0.014	0.023
Eldoret	-0.12	0.352	-0.01	0.307	0.015	0.03	0.29	0.018	0.025	0.000	1.0	0.0
Laikipia	0.268	0.181	0.096	0.268	0.181	0.033	0.03	0.894	0.007	0.067	0.757	0.013
Meru	0.206	0.075	0.022	0.053	0.656	0.004	-0.1	0.450	-0.01	-0.02	0.859	0.000
Kisumu	0.106	0.351	0.012	0.290	0.010	0.024	0.41	0.000	0.032	0.049	0.672	0.005
Kisii	0.299	0.011	0.028	0.285	0.017	0.026	0.40	0.001	0.026	0.185	0.125	0.015
Kericho	0.479	0.000	0.06	0.321	0.010	0.049	0.55	0.000	0.067	0.197	0.149	0.02
Nyeri	0.381	0.001	0.041	0.218	0.069	0.03	0.26	0.029	0.026	0.312	0.009	0.026
Embu	0.234	0.048	0.022	0.236	0.045	0.039	0.09	0.454	0.014	0.284	0.016	0.026
Garassa	-0.08	0.532	-0.01	0.09	0.467	0.009	0.16	0.172	0.01	-0.12	0.334	-0.01
Narok	-0.10	0.404	-0.02	0.016	0.900	0.004	0.17	0.145	0.015	-0.11	0.346	-0.01
Wilson	0.124	0.357	0.012	0.131	0.329	0.016	0.18	0.183	0.019	0.093	0.501	0.01
Dagorriti	0.030	0.799	0.003	0.121	0.287	0.012	0.13	0.240	0.012	0.141	0.218	0.01
JKIA	0.254	0.066	0.04	0.212	0.118	0.033	0.20	0.152	0.015	0.210	0.319	0.024
Kabete	0.080	0.483	0.008	0.020	0.870	0.002	0.31	0.006	0.025	0.177	0.122	0.015
Thika	0.217	0.080	0.028	0.402	0.001	0.055	0.37	0.004	0.044	0.322	0.012	0.046
Machak	0.227	0.062	0.024	0.169	0.172	0.017	0.38	0.002	0.037	0.270	0.027	0.025
Makindu	0.282	0.011	0.033	0.287	0.010	0.038	0.41	0.000	0.033	0.450	0.000	0.035
Lamu	0.277	0.012	0.01	0.602	0.000	0.051	0.64	0.000	0.044	0.479	0.000	0.033
Voi	0.147	0.209	0.017	0.169	0.153	0.018	0.07	0.548	0.004	0.089	0.453	0.009
Mtwapa	0.216	0.100	0.013	0.378	0.004	0.024	0.32	0.016	0.021	0.321	0.016	0.021
Malindi	0.570	0.000	0.035	0.579	0.000	0.059	0.64	0.000	0.055	0.468	0.000	0.039
Msabah	0.181	0.116	0.007	0.320	0.005	0.024	0.26	0.021	0.012	0.115	0.333	0.006
Mombasa	0.541	0.000	0.04	0.373	0.007	0.037	0.33	0.018	0.021	0.084	0.566	0.007

Mean monthly Tmin and Tmax for the individual station was also subjected to Mann-Kendall test. It was noticed that the station with Z-statistics greater than 0.28 had a statistically significant change at 5% significant level. Figure 2.16 and 2.17 shows the spatial distribution of the Z-statistics for each month for Tmax and Tmin respectively. On the spatial scale, only the month of May depicted a positive trend for Tmax which is statistically significant for all of the stations across the country. On the other hand, the month of May to November had a positive trend in most stations for Tmin which was significant. June to August months showed a significant increasing trend, which is statistically significant at $p < 0.05$ level in more than 90% of the stations analyzed, while the December, January, and February which are the hottest months, had an increasing trend which is not statistically significant. Overall there is an increase in night temperature more than that of warming during the day. This will likely lead to a decrease in human comfort.

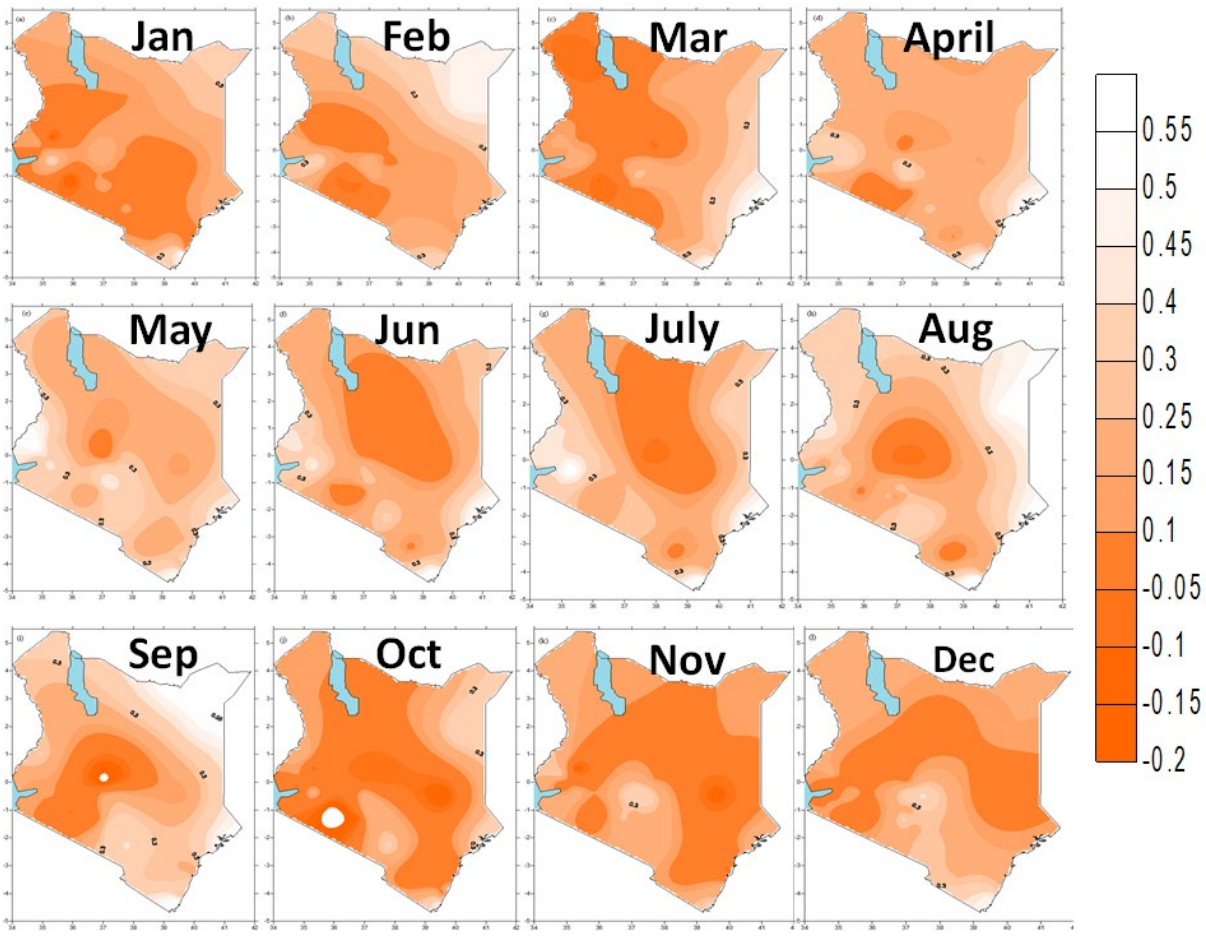

Figure 16 Spatial Distribution of monthly Man-Kendall (MKZ)statistics for Tmax

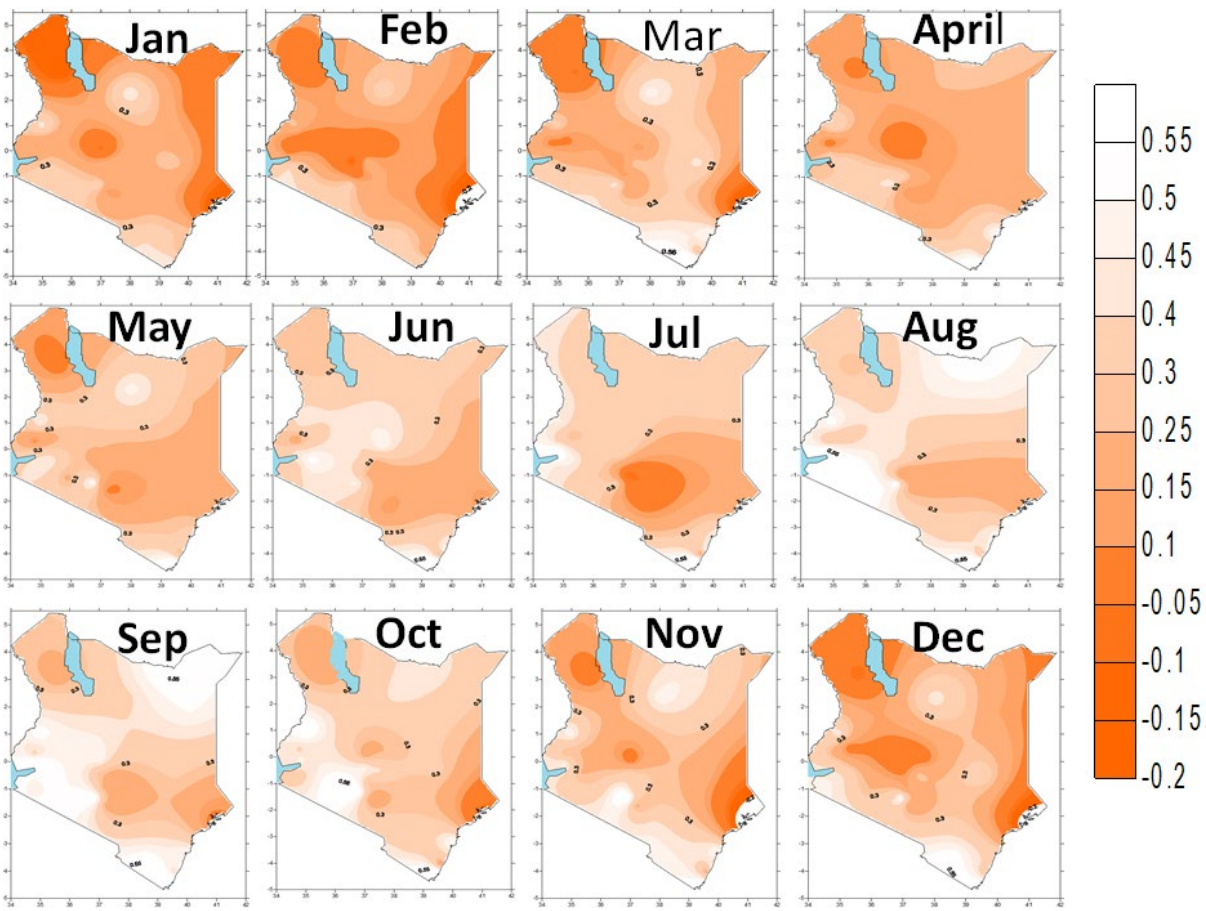

Figure 17 Spatial Distribution of Monthly Man-Kendall (MKZ) statistics for minimum temperature

2.5 Assessment of the RCMs' Skills in Simulating Large-Scale Signals

Kenyan rainfall is highly variable; it has a strong inter-annual and spatial variability, which is associated with extreme events (droughts and floods). Studies by Black et al. (2003), and Indeje et al. (2000) have clearly shown that inter-annual variability of rainfall in Kenya is associated with perturbation of global Sea Surface Temperature (SST). In particular, El Niño/La Niña (ENSO) and IOD phenomenon play a critical role in this variability. El Niño and positive IOD are associated with heavy rainfall and La Niña and negative IOD are associated with depressed rainfall over Kenya (Mutemi, 2003). Interannual rainfall variations in Kenya is highly linked to the El Niño Southern Oscillation (ENSO), with more rain and flooding during El Niño and droughts in La Niña years, both having severe impacts on human habitation and food security.

Figure 2.18 shows the location used to compute different Niño index. In this study Niño 3.4 was used for ENSO which is sea surface temperature anomaly (SSTA) averaged over (150° W-90°W, 5°S- 5°N) and Dipole Mode Index (DMI) was used for IOD, which is defined as the difference between western Indian ocean box (50° E-70°E, 10°S- 10°N) and Eastern Indian ocean box (90° E-110°E, 10°S- Equator). Composite analysis method was used to understand the ability of the models in simulating teleconnection (ENSO and IOD) which are associated with Kenyan rainfall. In this method, composite for pure El Niño Southern Oscillation (ENSO), pure Indian Ocean Dipole (IOD) and co-occurrence of ENSO and IOD events are formed separately to understand the RCMs response in each case.

Identification of ENSO and IOD years was done by the SSTA from January 1960 to December 2016 period. Figure 2.19 shows that Niño 3.4 and IOD are independent of each other. The strongest IOD is seen in 1960, 1961, 1992 and 2011, and it is not followed by ENSO phenomena. On the other hand, the strongest ENSO is seen in 1965, 1987, and 1988, and it is not followed by IOD phenomena (figure 4.29). In addition, there are several years when IOD and ENSO occur concurrently, such as 1963, 1972, 1982,1997 and 2015. Table 4.11 summaries the years of pure El Niño (La Niña), positive(negative) IOD and co-occurrence of the two events. The years in table 4.11 were used to assess the ability of the model in capturing the variability caused by the two events. The selected years were composites for each phenomenon. Table2.3 shows that the co-occurrence take place between positive IOD and El Niño, and Negative IOD and La Niña. And there are several years of such events. Positive IOD and La Niña and Negative IOD and El Niño never occur.

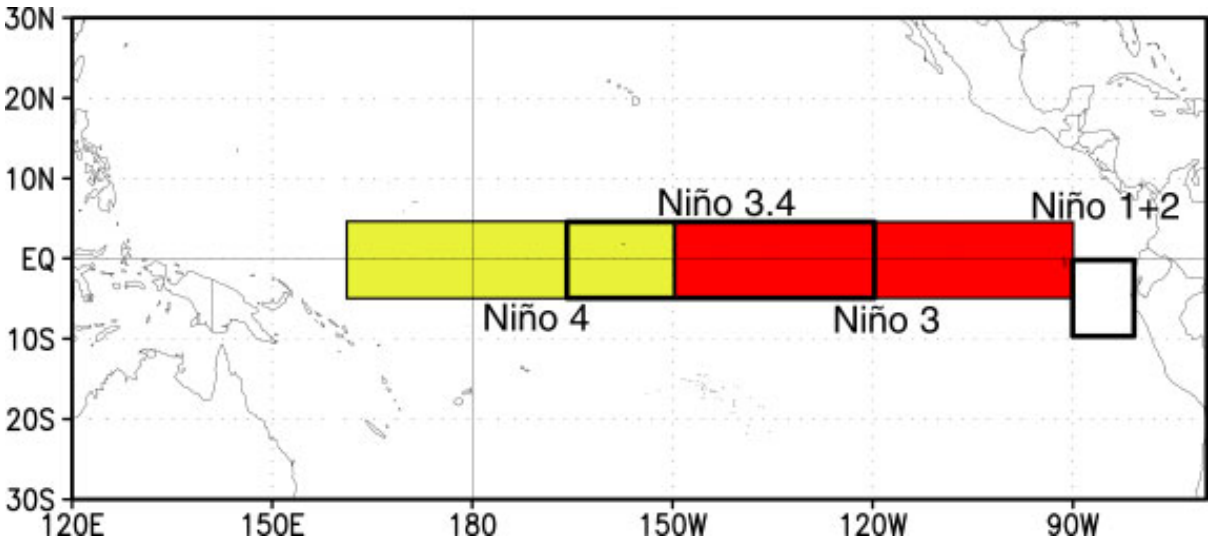

Figure 18 Graphical depictions of the four Niño regions (source: CPC: http://www.cpc.noaa.gov/products/analysis_monitoring/ensostuff/nino_regions.shtml)

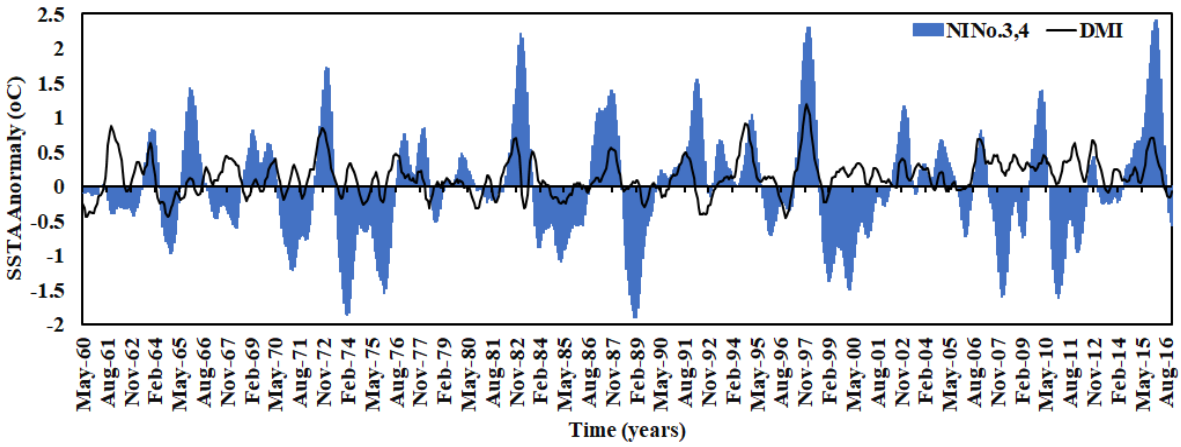

Figure 2.19 Index of IOD and Nino 3.4 during January 1960 to December 2016 period. Positive (Negative) Anomaly Shows El Niño (La Niña) event and Positive (Negative) IOD.

Table 5 The years of IOD, ENSO and the co-occurrence of both

	El Nino	Normal	La Nina
Positive IOD	1963, 1972, 1982, 1997	1961, 1967	-
Normal	1965, 1986, 1987, 2002, 2009	1978, 1979, 1990, 1993, 1995	1970, 1971, 1973, 1988, 1999, 2007
Negative IOD	-	1960, 1996	1998

Sea surface temperature variability during OND and MAM season is shown in figure 2.20. The ENSO and IOD signals are very clear during OND season but only ENSO signal persists to MAM season of the following year. During Positive IOD and El Niño years, the SST over Western Indian Ocean is warmer than the Eastern Indian Ocean and Colder during La Niña and negative IOD events. The warmer SST provide the moisture that results to enhance rainfall during Positive IOD and El Niño years. Rainfall over Kenya is Positively correlated to SST over the western Indian Ocean and negatively correlated to the southeastern Indian Ocean SST (Figure 2.21). Over the Pacific, it is positively correlated at the Central and eastern Pacific which are the NINO regions that are used for ENSO Index calculation. The SST gradient in the Indian Ocean is Key to enhanced (depressed) rainfall over Kenya during the OND season.

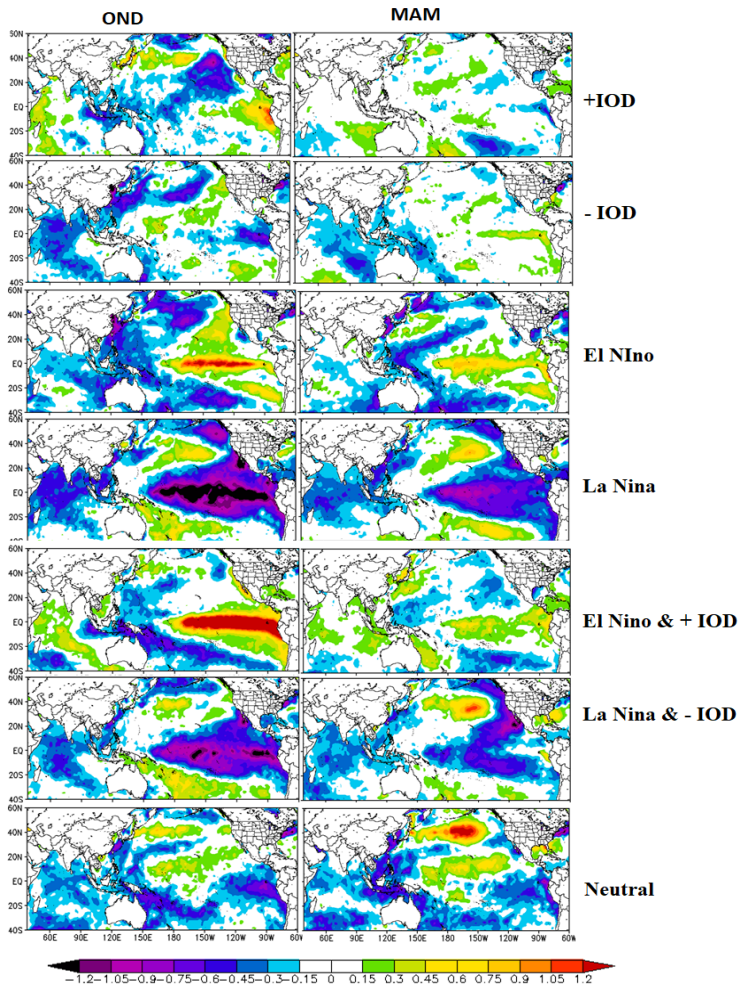

Figure 19 Composite of SST anomaly (ºC) during OND and MAM, on (a) Positive IOD, (b) Negative IOD, (c) El Niño, (d) La Niña (e) Positive IOD and El Niño, (f) Negative IOD and La Niña, and (g) No IOD and No ENSO. Positive (negative) value shows the increasing (decreasing) of SSTs.

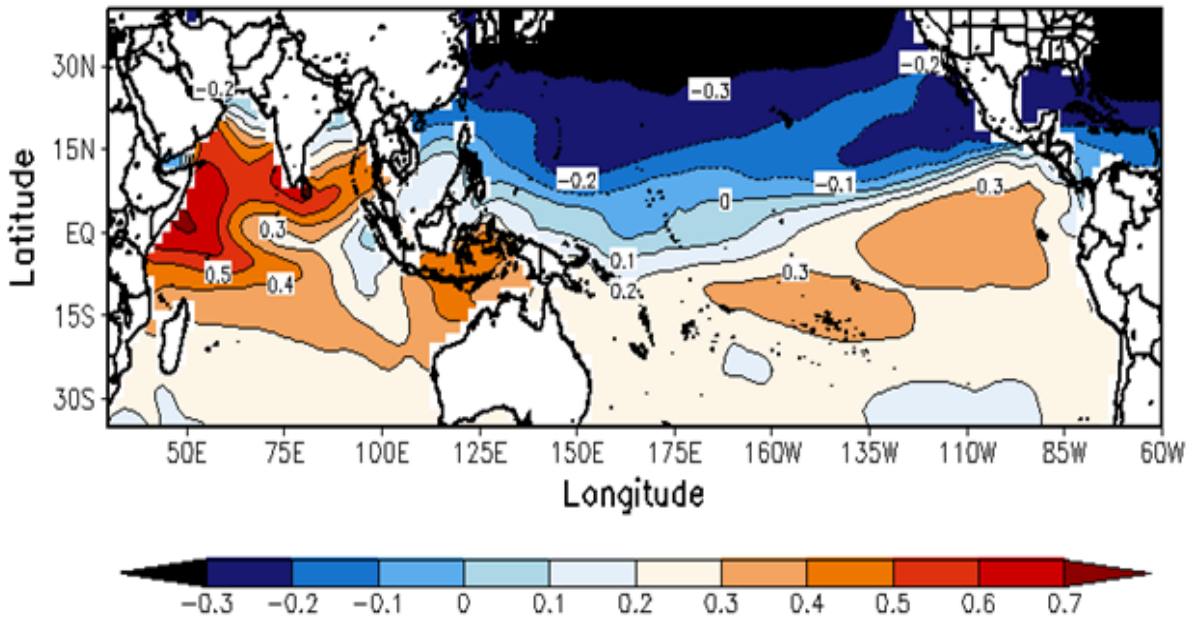

Figure 20 Spatial correlation of Kenyan rainfall to the Sea surface temperature

From the Observed dataset, it is clear that there is no clear influence of ENSO and IOD in the spatial distribution of rainfall pattern over Kenya during MAM season (figure 2.21). whereas, for OND season enhanced (heavy) rainfall is observed when we have positive IOD, El Niño and co-occurrence of the two events. On the other hand, depressed rainfall is observed in years of negative IOD, La Niña and co-concurrence of the two (Figure 2.20). This concurs with previous studies that concluded that enhanced (depressed) rainfall during OND season is much associated with ENSO and IOD variability and no much influence of the two events to MAM season. Generally, from figure 2.22 and 2.23, OND season is influenced by the ENSO and IOD and that shows there is a high possibility of above normal rainfall over Kenya during the pure El Niño event, positive IOD and when they co-occur. La Niña and negative IOD are associated with dry conditions over Kenya during OND season. Therefore, a high risk of the dry condition during the negative IOD and when they co-occur with La Niña.

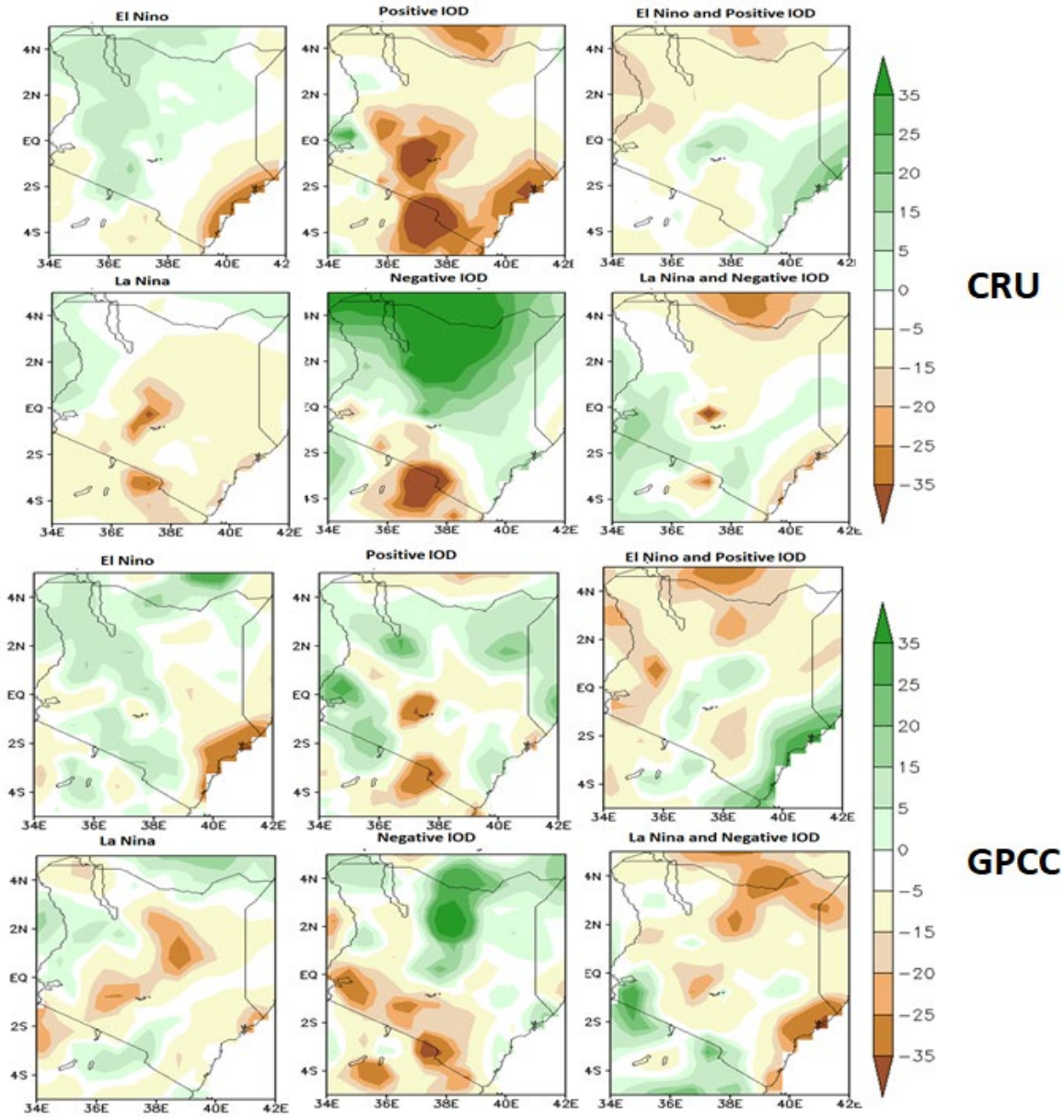

Figure 21 Composite rainfall anomalies during MAM season for CRU and GPCC data for the classification years listed in (Table 4.11).

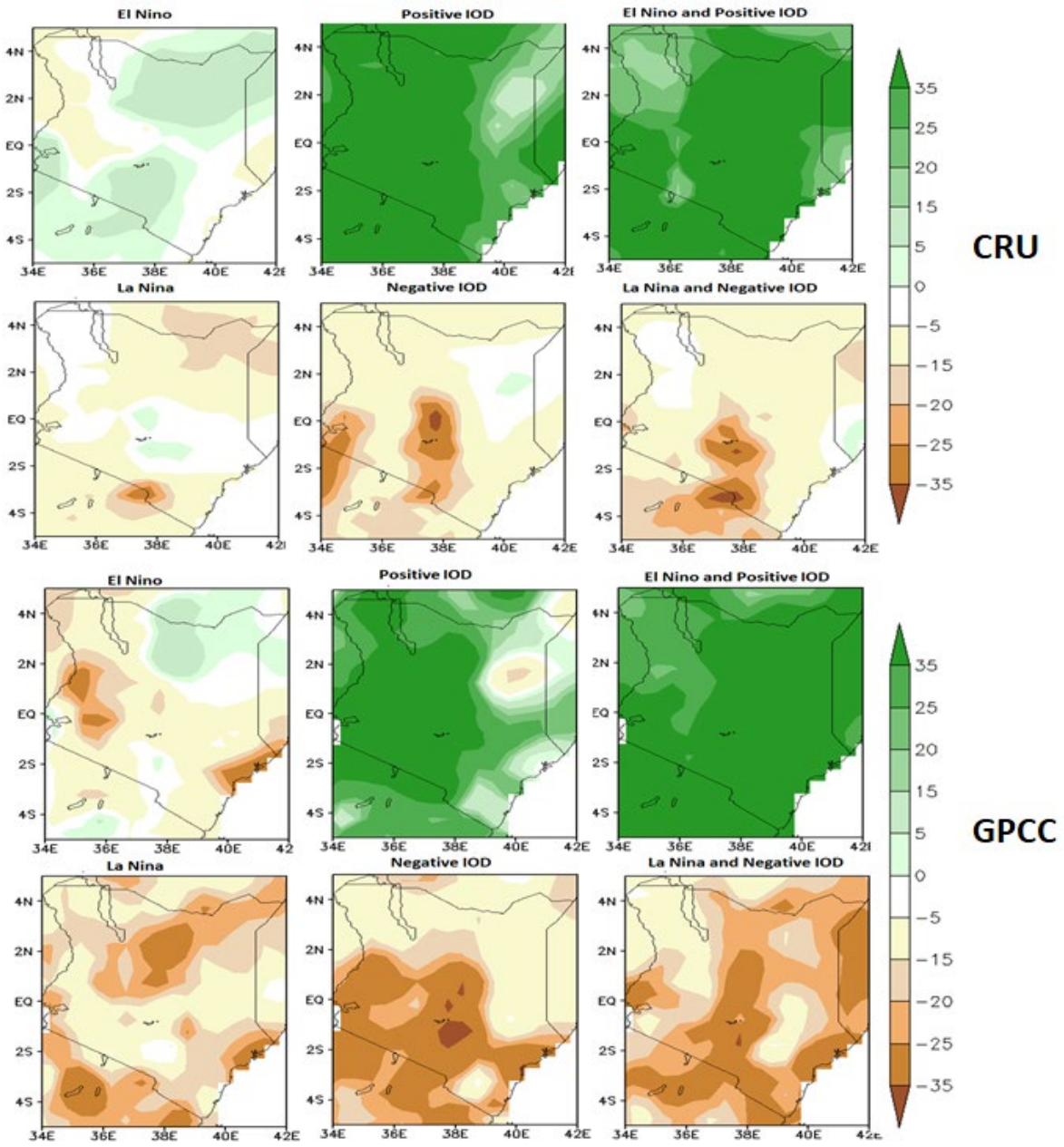

Figure 22 Composite rainfall anomalies during OND season for CRU and GPCC data for the classification years listed in (Table 4.11).

2.6 Analysis of Future Projections of Temperature and Rainfall over Kenya

Due to the high spatial variability of rainfall and temperature over Kenya. The country was subdivided into twelve homogeneous zones across Kenya (Figure 2.23). The stations within each homogeneous zone were used to represent the entire country (table 2.4). In demarcating the homogeneous zones, they used empirical orthogonal function (EOF) technique to map out a network of rainfall station over Kenya into homogeneous zones. The used the zones for further understating how the future changes are likely to take place.

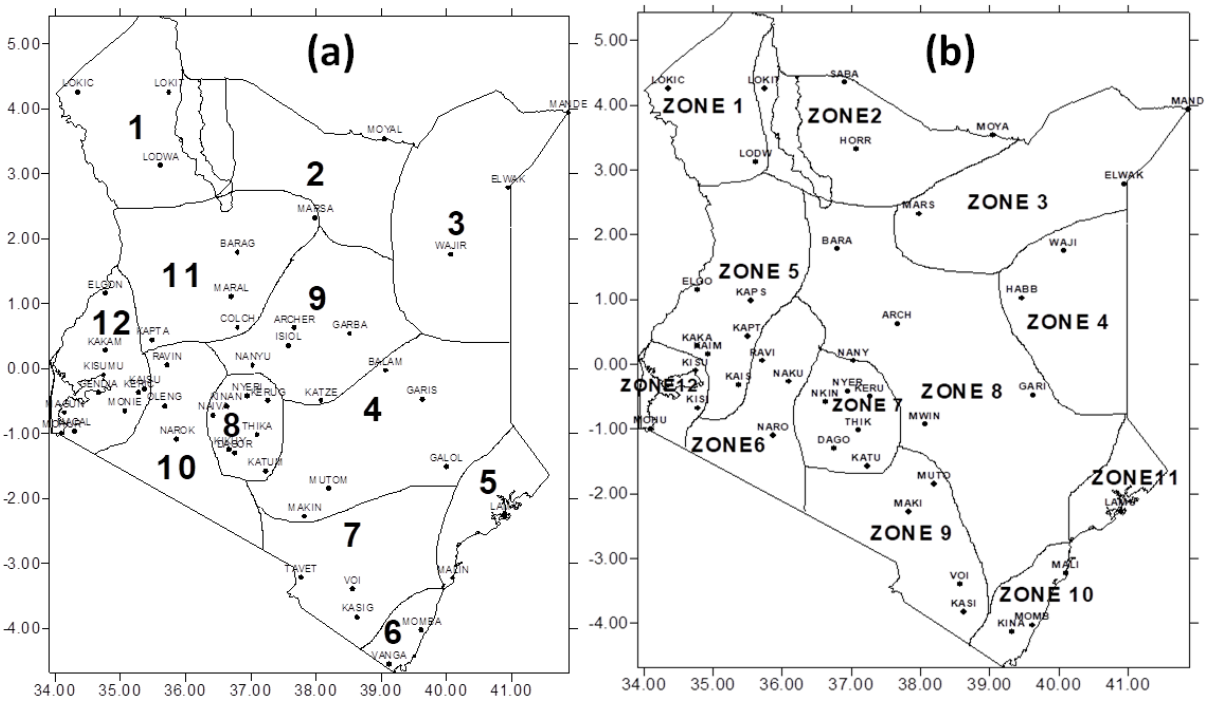

Figure 23 Homogeneous rainfall zones over Kenya for (a) MAM and (b) OND seasons. Source: Rainfall Atlas (Authors: Muhindi, Ndichu, and Oloo, Kenya Meteorological Dept, 2001)

Table 6 Rainfall stations used for each Homogeneous zone in the Study and their Coordinates for (a) MAM and (b) OND Seasons

(A)

Station ID	Station	Lat (°)	Lon (°)	Elevation (m)	Zone
Lod	Lodwer	3.7	35.37	506	1
Moy	Moyale	3. 32	39.02	1097	2
Waj	Wajir	1.45	40.04	244	3
Gar	Garissa	-0.29	39.38	147	4
Lam	Lamu	-2.16	40.54	30	5
Mom	Mombasa	-4.02	3937	55	6
Voi	Voi	-3.24	38.34	597	7
Dag	Dagoretti	-1.18	36.45	1798	8
Nan	Nanyuki	0.03	37.02	1905	9
Nar	Narok	-1.08	35.5	1890	10
Mar	Marsabit	2.18	37.54	1345	11
Kis	Kisumu	-0.06	34.45	1145	12

(B)

Station ID	Station	Lat (°)	Lon (°)	Elevation (m)	Zone
Lod	Lowder	3.7	35.37	506	1
Moy	Moyale	3.32	39.02	1097	2
Man	Mandera	3.56	41.52	230	3
Waj	Wajir	1.45	40.04	244	4
KAK	Kakamega	0.17	34.47	2133	5
Nak	Nakuru	-1.16	36.06	1901	6
Dag	Dagoretti	-1.18	36.45	1798	7
Gar	Garissa	-0.29	39.38	147	8
Voi	Voi	-3.24	38.34	597	9
Mom	Mombasa	-4.02	39.37	55	10
Lam	Lamu	-2.16	40.54	30	11
Kis	Kisumu	-0.06	34.45	1146	12

2.7 Changes in Future Rainfall under RCP 4.5 and RCP8.5 Scenarios over Kenya.

Figure 2.24 to 2.25 show the projected MAM seasonal rainfall change as projected by RACMO, CCLM, HIRHAM, CCLM, RCA and REMO over Kenya, for 2021 -2100 under RCP4.5 and RCP8.5 scenario. Different models depict different scenarios in rainfall during the MAM season. RACMO, RCA, and REMO depict a wetter condition at the end of the century for RCP4.5, while CCLM and HIRHAM show a drier condition. Similar, for RCP8.5 reduced rainfall, is depicted in HIRHAM and CCLM, while RCA, REMO, and RACMO show wetter and drier in a different part of Kenya. Generally, for MAM the models indicate a reduced rainfall relative to the historical period 1961-2000.

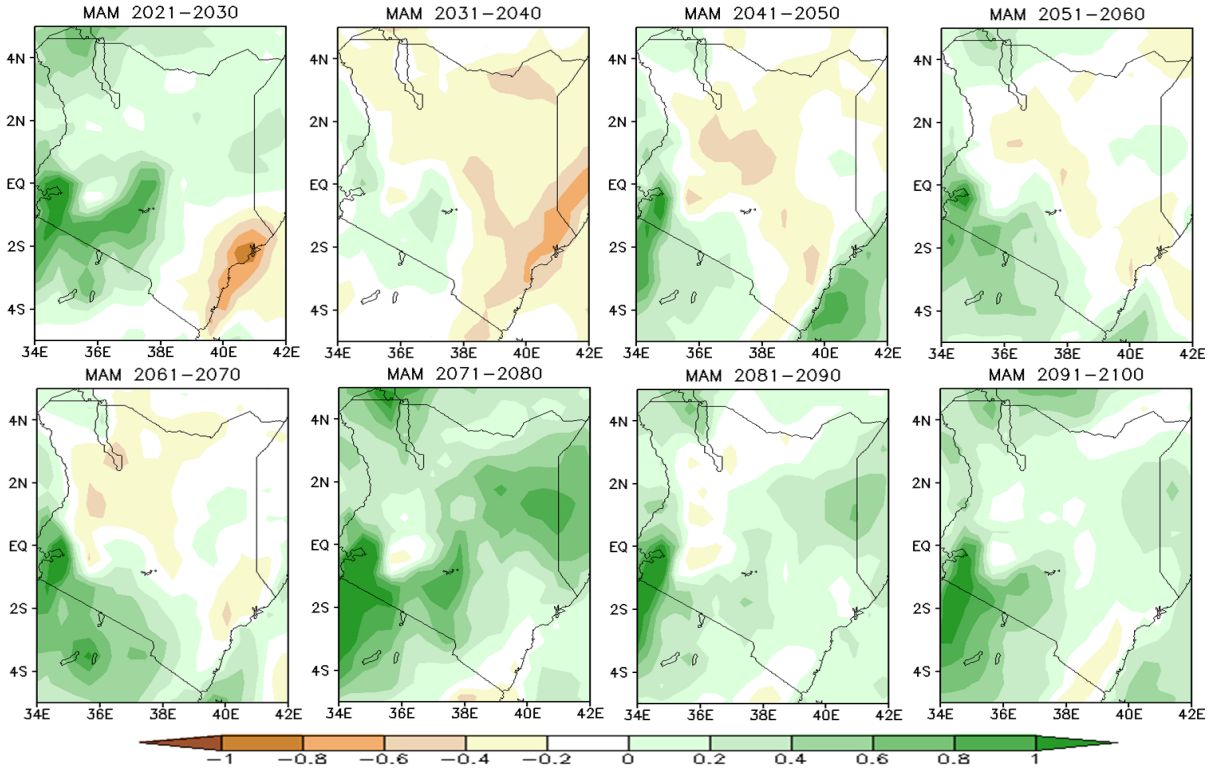

Figure 24 March-May seasonal rainfall change (mm) over Kenya as simulated by RACMO model under the RCP4.5 scenario, relative to the baseline period 1961–2000.

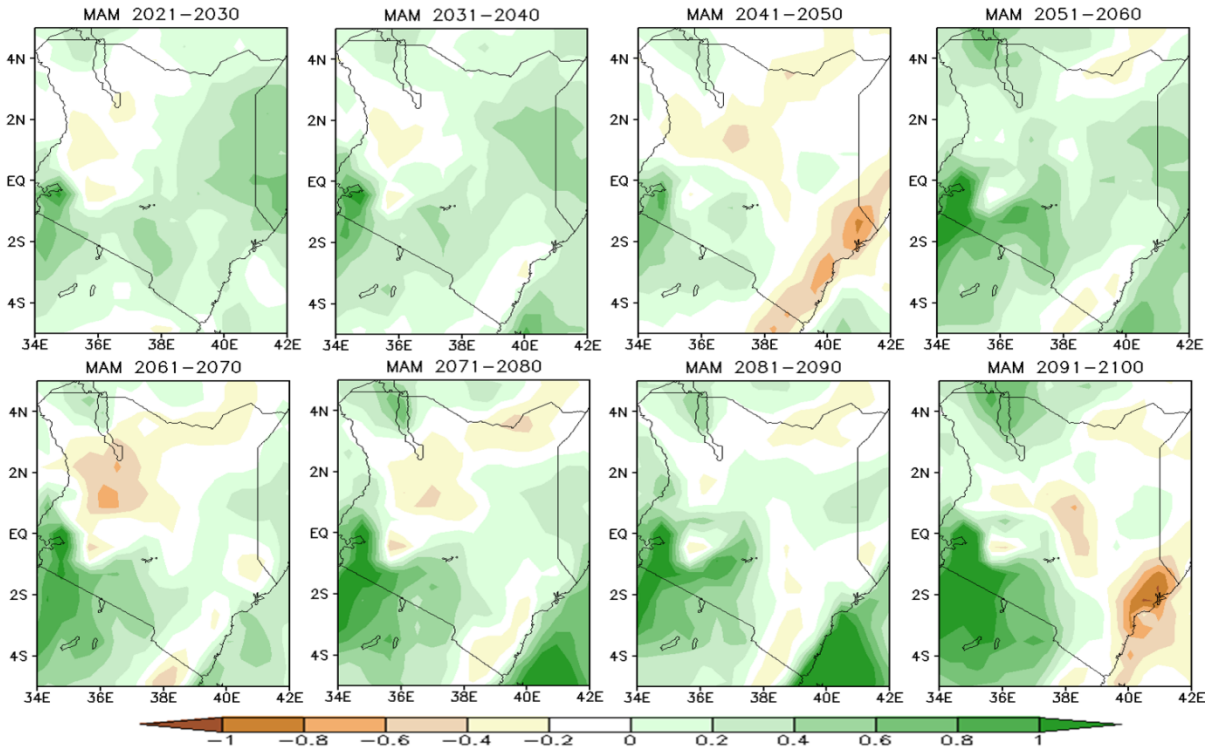

Figure 25 March-May seasonal rainfall change (mm) over Kenya as simulated by RACMO model under the RCP8.5 scenario, relative to the baseline period 1961–2000.

Figure 2.26 -2.27 show the projection of rainfall during the OND season by REMO, RCA, HIRHAM, CCLM and RACMO for 2020 -2100 Under RCP4.5 and RCP8.5 scenario. The wetter condition is projected over Kenya for both scenarios (RCP4.5 and RCP8.5). The projected wetter condition under RCP8.5 is greater than under RCP4.5. Most parts of the country is likely to receive enhanced rainfall during OND season, with exception of northwestern Turkana area as projected by the models. The wetness during the OND season has been linked to higher warming rates over the western Indian Ocean than over the eastern Indian Ocean, therefore high chances of occurrence of positive IOD, which is generally linked to enhanced rainfall over Kenya during OND season (Shongwe et al., 2011).

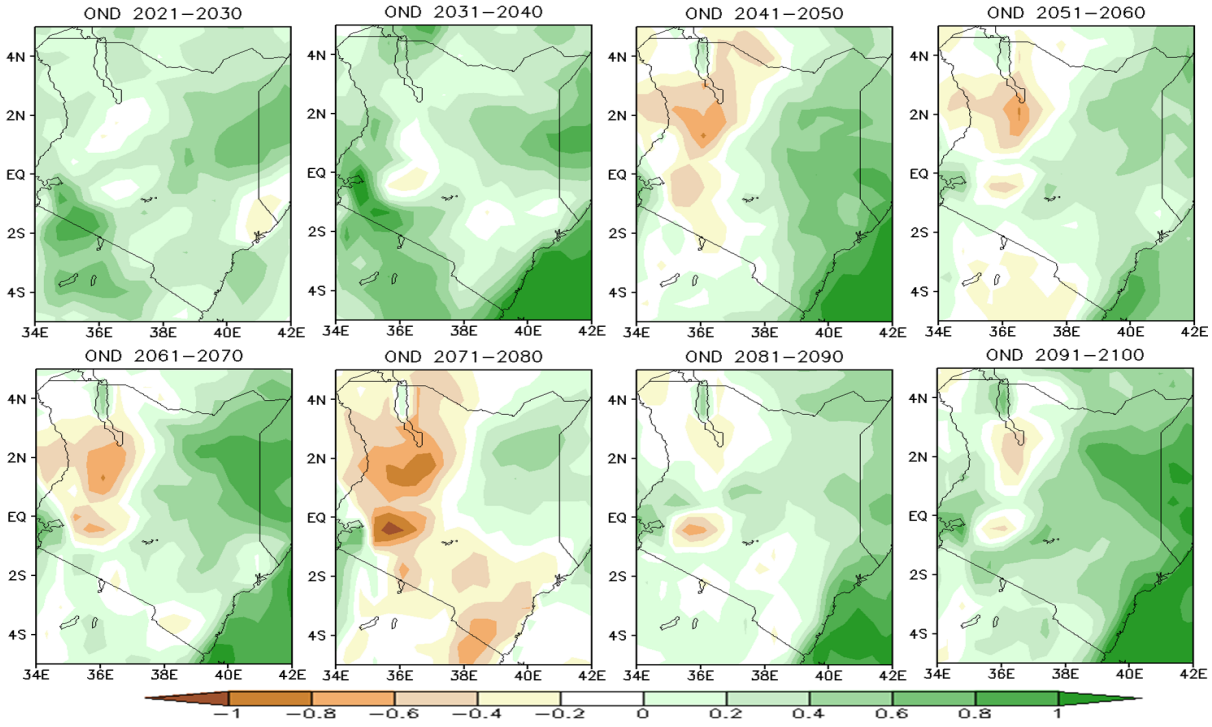

Figure 26 Figure 2.26 October-December seasonal rainfall change (mm) over Kenya as simulated by RACMO model under the RCP4.5 scenario, relative to the baseline period 1961–2000.

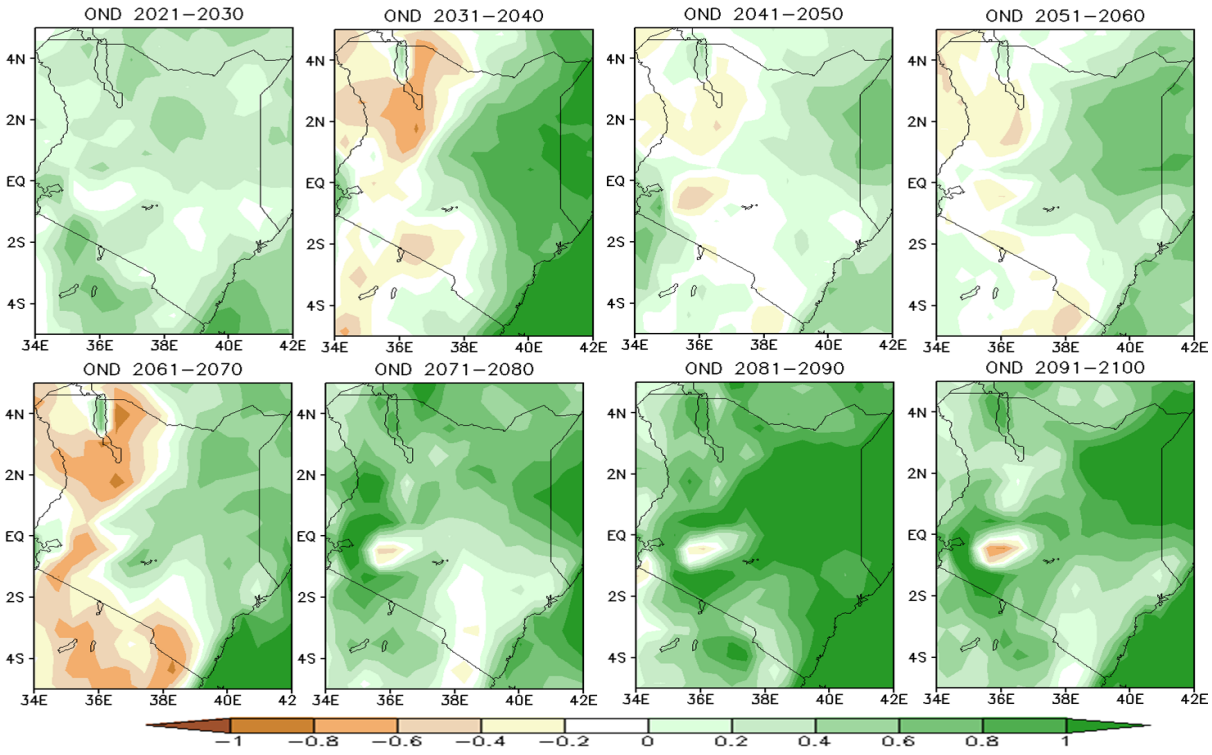

Figure 27 October-December seasonal rainfall change (mm) over Kenya as simulated by RACMO model under the RCP8.5 scenario, relative to the baseline period 1961–2000.

Figure 2.27. The indication and the magnitude of the change in rainfall for a period of 2021-2100 over Kenya are presented in Table 4.13. REMO and CCLM project a decrease in rainfall during MAM and OND seasonal rainfall. The decrease in MAM is statistically significant for 5% significant level while the decrease in OND is insignificant. For REMO the decrease is insignificant for both MAM and OND seasonal rainfall. HIRHAM project a decrease in MAM and increase in OND with an increase in the annual rainfall for both RCP4.5 and RCP8.5, which is statistically significant at project 10% significant level, the increase in annual rainfall is mainly due to a statistically significant increase in OND at 5% significant level. RCA and RACMO project an increase in both MAM and OND rainfall which is also statistically significant. All the models project an increase in rainfall during OND season under RCP8.5 and annual increase, except CCLM which project decrease in annual rainfall over Kenya under RCP8.5. The indication is MAM seasonal rainfall is likely to be reduced while that of OND season is likely to increase Under RCP8.5. Under RCP8.5 it is clear that the increase is expected for OND season, however, under RCP4.5, three models indicate a reduction in OND rainfall which is statistically insignificant. For the annual rainfall, a statistically significant increase is shown by Four models, Two under RCP4.5 and two under RCP8.5 (Figure 27).

2.8 Future Temperature Change over Kenya.

Figure 2.28 -2.29 show the projected change in maximum and minimum temperature as projected by the ensemble CORDEX model for 2020 to 2100 relative to the climatological period 1971 -2005 under RCP4.5 and RCP8.5 scenarios. The last half of the 21st century is likely to be warmer than that of 2020 -2050 for both minimum and maximum temperatures and under the two scenarios. The expected temperature rise under RCP8.5 is more than that of RCP4.5. For maximum temperature, the increase is likely to range between 0.2 and 3.4 ^{o}C under scenario RCP4.5 and between 0.8 and 4.8 ^{o}C under RCP8.5 (Figure 2.28 -2.29). On the other hand, the minimum temperature is increasing between 0.2 to 2.8 ^{o}C and 1.6 to 5.5 ^{o}C under scenario RCP4.5 and

RCP8.5 respectively (figure 2.30 and 2.31). The warming is likely to be more over the northwestern part of the country in both minimum and maximum temperature under the two scenarios. Also, the increase in minimum temperature is more than that of maximum temperature.

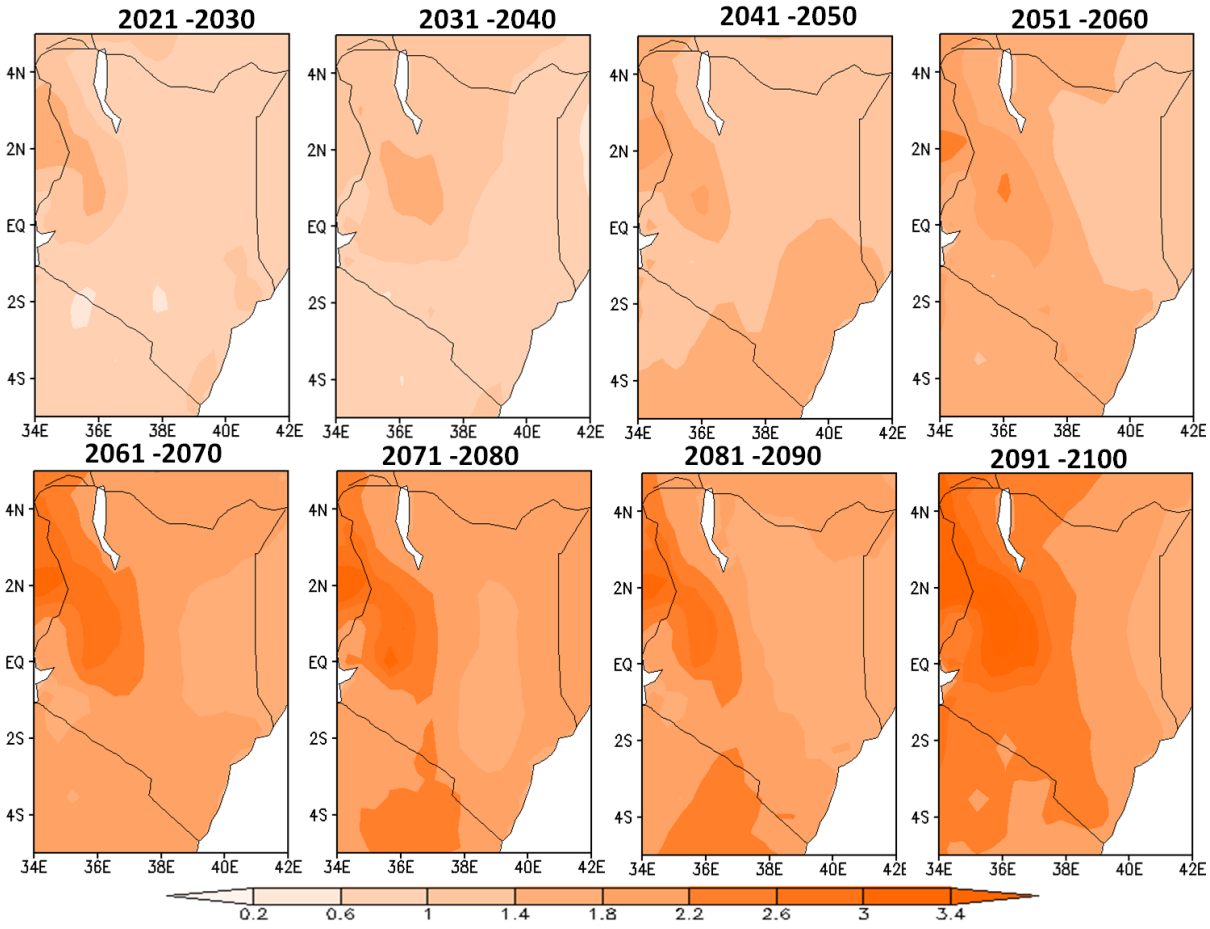

Figure 28 Maximum temperature change (°C) projected by ensembled model under RCP4.5 from 2021 to 2100.

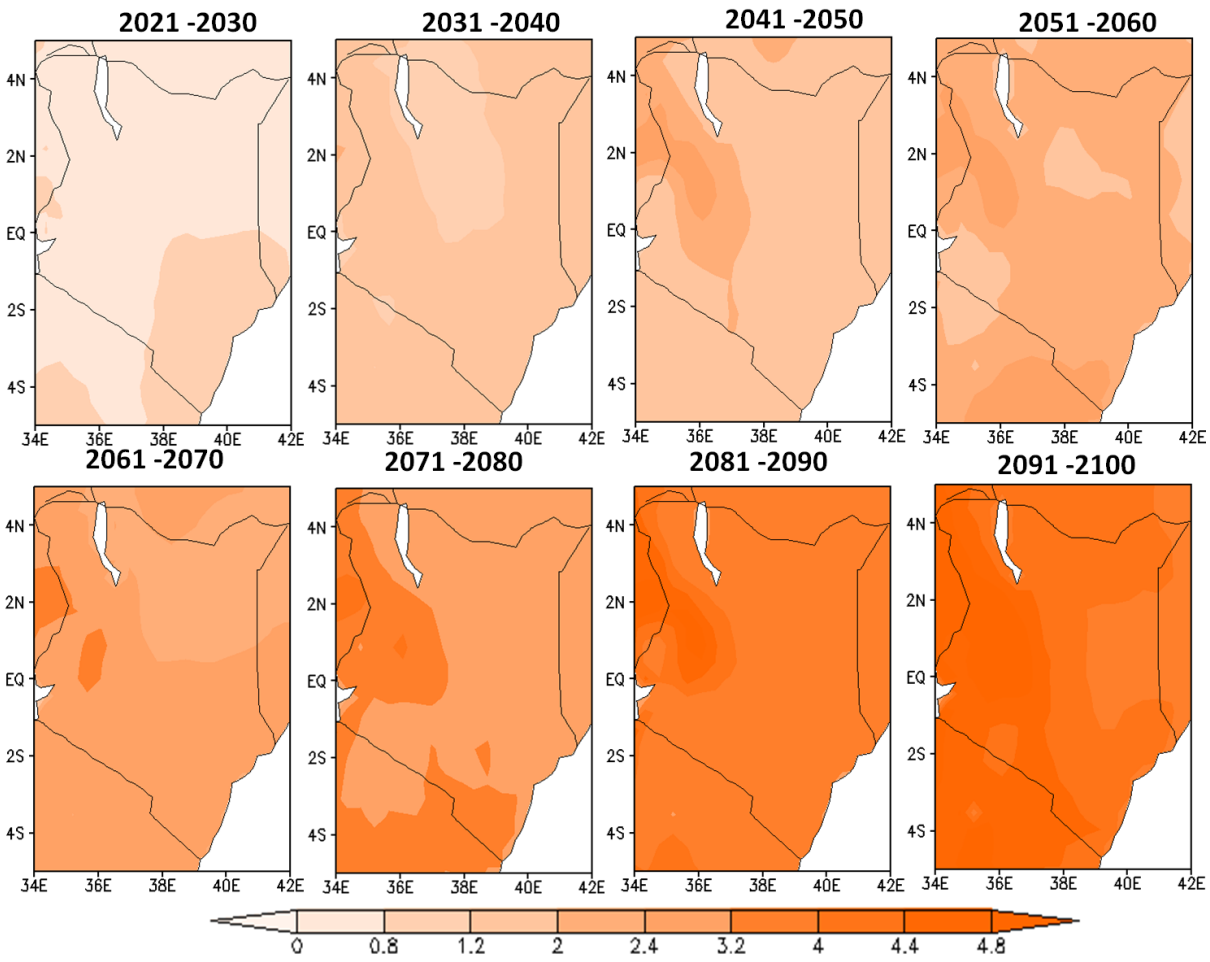

Figure 29 Maximum temperature change (°C) projected by ensembled model under RCP8.5 from 2021 to 2100.

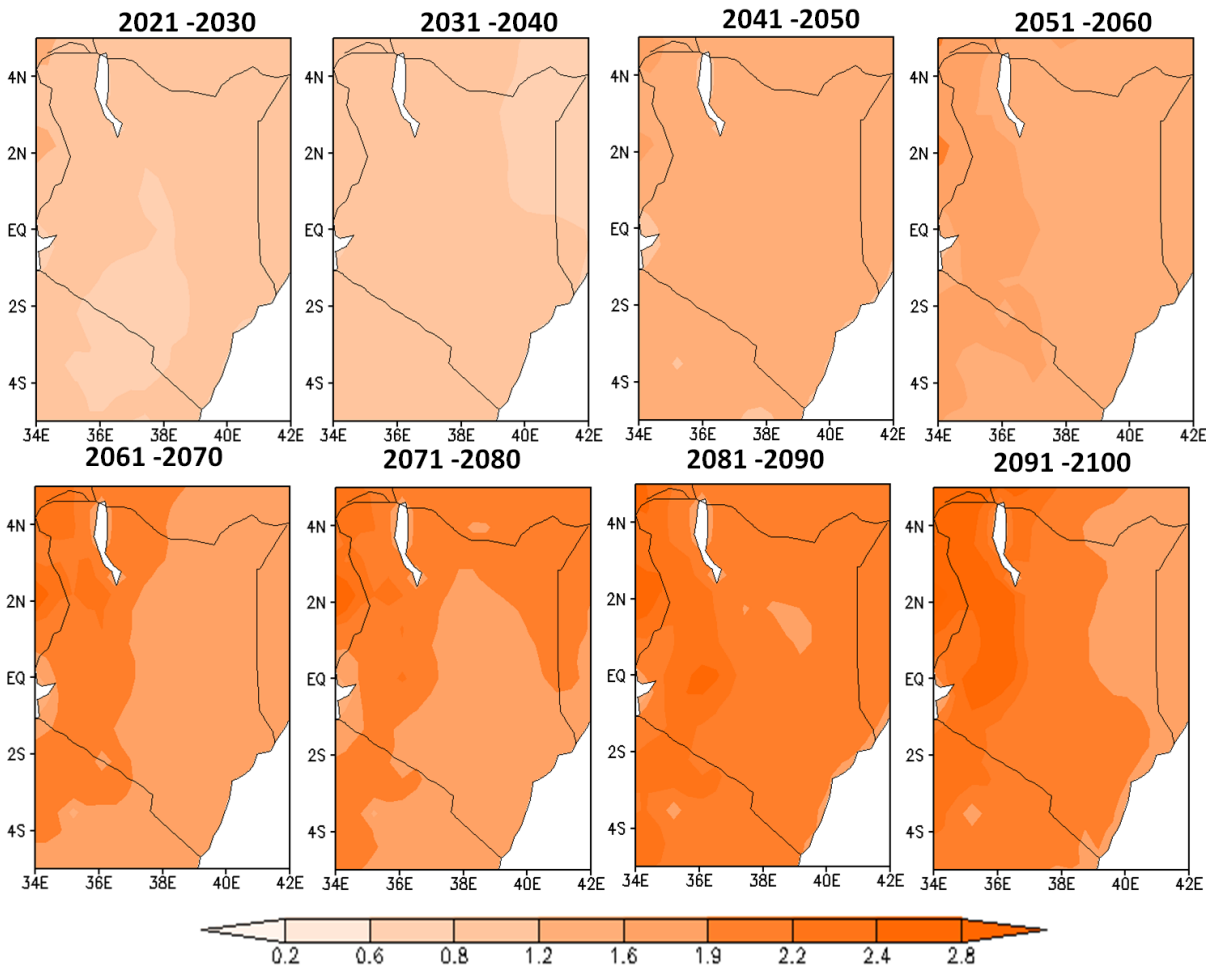

Figure 30 Minimum temperature change (°C) as projected by ensembled model under RCP4.5 from 2021 to 2100.

Figure 2.30

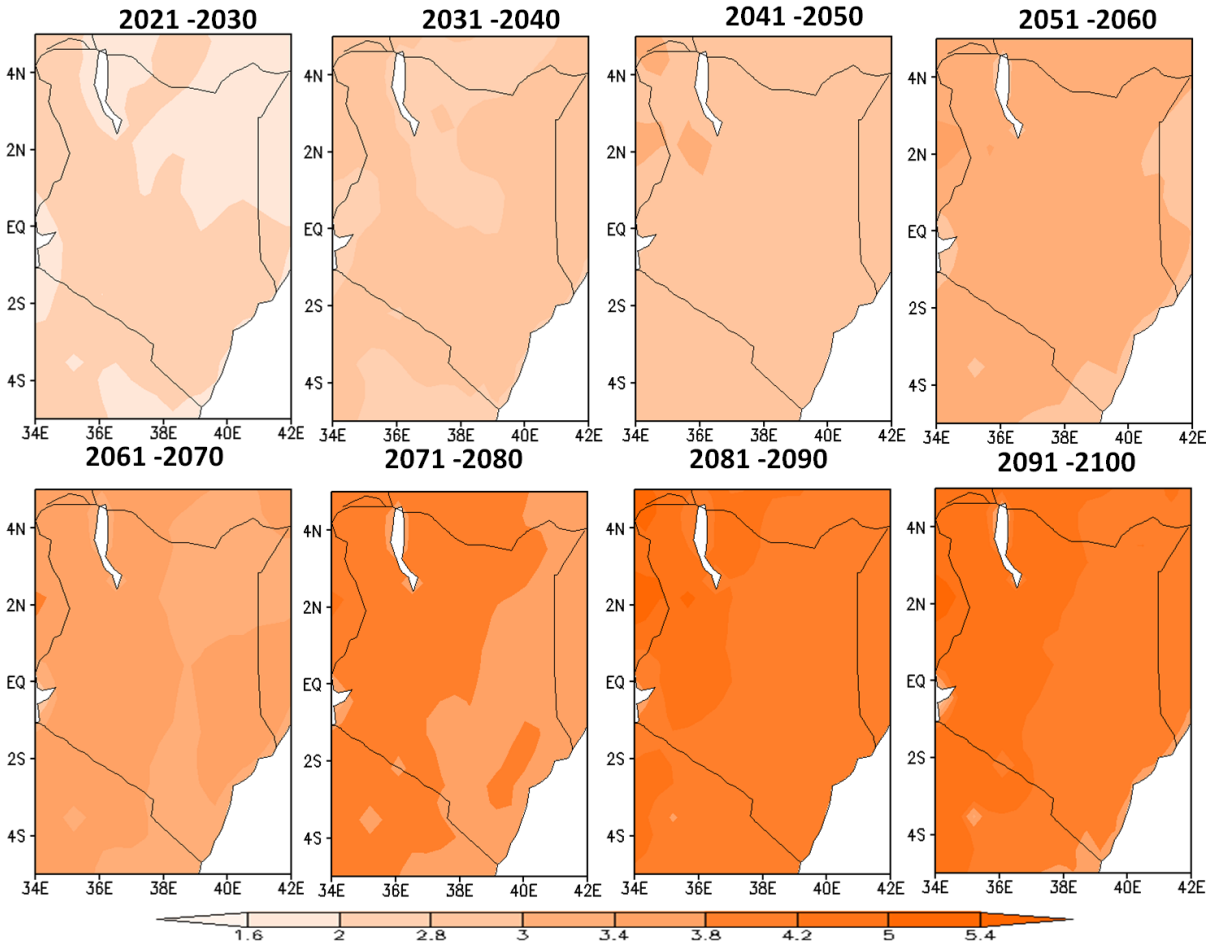

Figure 31 Minimum temperature change (°C) as projected by ensembled Model under RCP8.5 from 2021 to 2100.

3.0 Simulated Future Change in Climate Extreme Events over Kenya

Figure 2.32 shows the time series of temperature extreme indices for three CORDEX models (CCLM, HIRHAM, and RACMO) under the RCP4.5 and RCP8.5. It shows that cool day (TX10) and cool night (TN10) show a downward trend toward the end of the 21st century under both RCP4.5 and RCP8.5. There is no much change in DTR for the HIRHAM model, while RACMO shows a declining trend and CCLM show a high variability IN DTR especially RCP4.5. Warm night (TN90) Warm days (TX90) are increasing with TX90 under RCP4.5 showing high variability for all the models. Finally, warmest night (TNx) and hottest day (TXn) are also on the rise with minimal variability. minimum temperature extreme (TNx and TNn) indices have a steeper slope than those of maximum temperature (TXx and TXn), similarly, the indices that are associated with cold extremes have weaker trend and gentle slope than those that are associated with warm extremes (TX90p and TN90p) (figure 2.32). All the models agreed on the general tendency of future projections of temperature extreme indices.

.

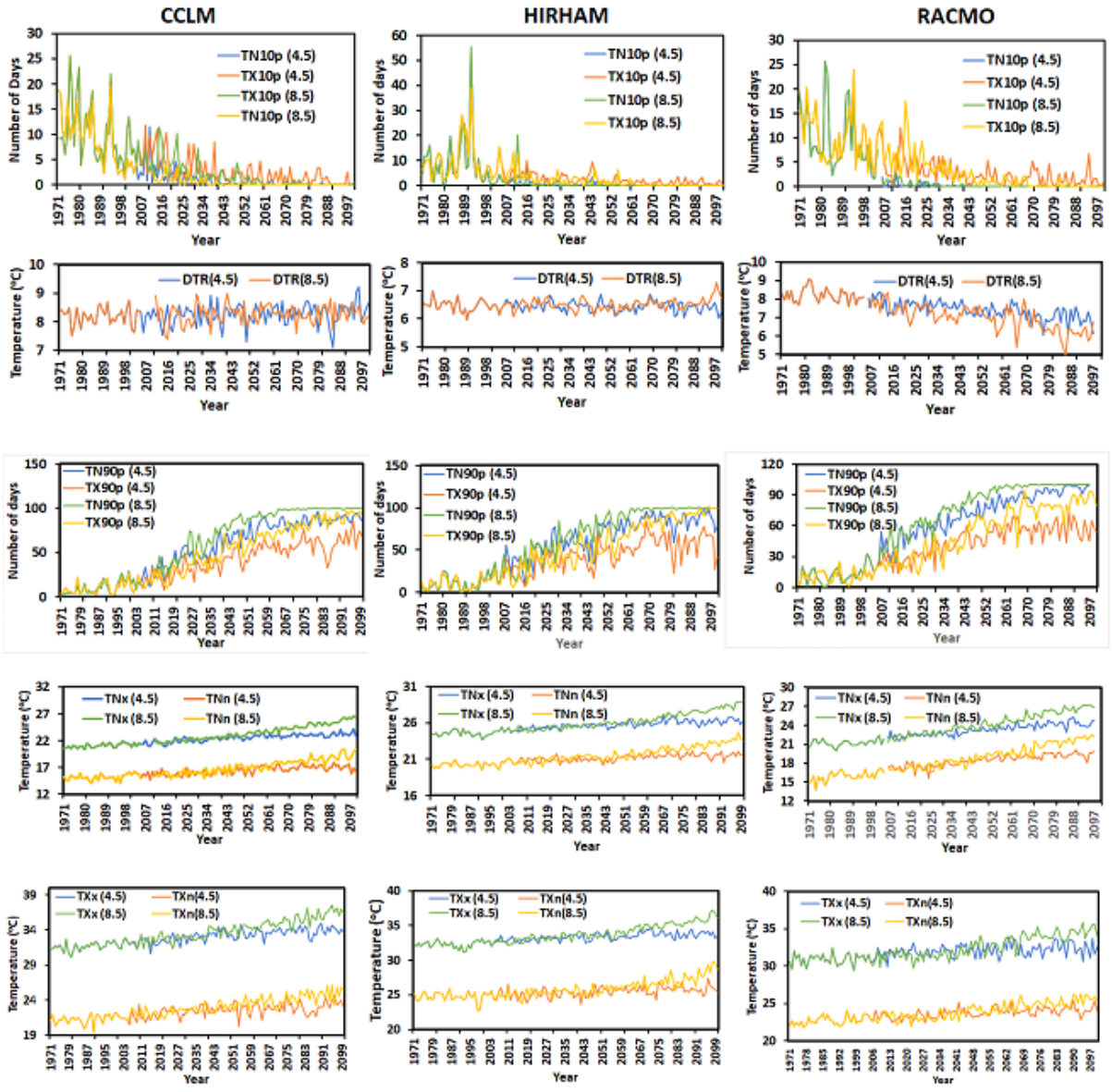

Figure 32 Annual time series of temperature extremes for Kenya as predicted by the three CCLM, HIRHAM, and RACMO RCMs.

4.0 Changes in Future Rainfall under RCP 4.5 and RCP8.5 Scenarios over Kenya

Future projected changes in rainfall over Kenya were assessed for near- (2011-2040), mid- (2041-2070), and far- (2071-2100) future climates relative to the current climate (1976-2005) using CORDEX-Africa regional climate model (RCM) runs forced by GCM simulations under three emission scenarios (RCP2.6, 4.5, 8.5).

Based on assessment of the performance of 24 model runs from five CORDEX-EA simulations, Ogega et al (2020) identified four RCM runs that outperform the all-model or individual model ensemble means in describing the spatio-temporal characteristics of precipitation over Eastern Africa. Accordingly, the top four performing runs are the REMO2009 forced by MPI-M-MPI-ESM-LR GCM for r1i1p1 ensemble member, SMHI Rossby Center Regional Atmospheric Model (RCA4) driven by the r1i1p1 members of CNRM-CERFACS-CNRM-CM5 and MPI-M-MPI-ESM-LR GCMs, and RCA4 driven by r2i1p1 member of MPI-M-MPI-ESM-LR GCM.

All four models data were used for the present assessment of projected precipitation changes over Kenya under RCP8.5 scenarios, but only three of the models with r1i1p1 ensemble members were available to assess projected changes under the RCP4.5 scenarios.

Figures 33 and 34 show the projected decadal MAM seasonal rainfall changes (mm/day) over Kenya based on the ensemble means of the best four model runs under RCP 4.5 and RCP 8.5 scenarios. Although there are spatial variability over the 8 future decades, there is generally a reduction in projected seasonal rainfall over northern Kenya and increase over southern regions for both RCP4.5 (Fig. 24) and RCP 8.5 (Fig. 25) scenarios compared to the 1960-2000 present climate simulations of best-model ensemble mean. Except for MAM 2081-2090 decadal rainfall change, the projected reduction appears to intensify and expand southwards under the RCP 8.5 scenario.

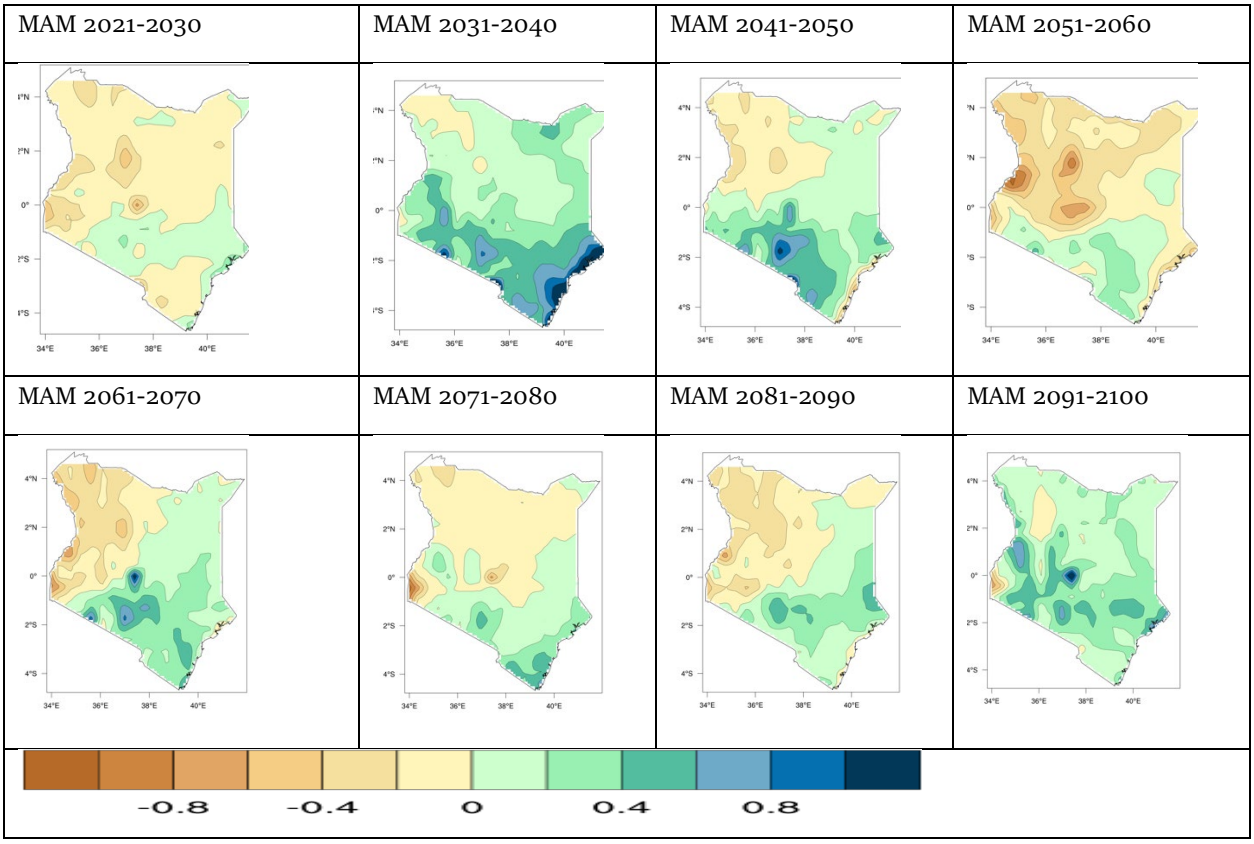

Figure 33: March-May seasonal rainfall changes (mm/day) over Kenya obtained from ensemble means of four top performing RCMs under the RCP4.5 scenarios for future ten-year periods from 2021 relative to historical simulations for the period 1961–2000.

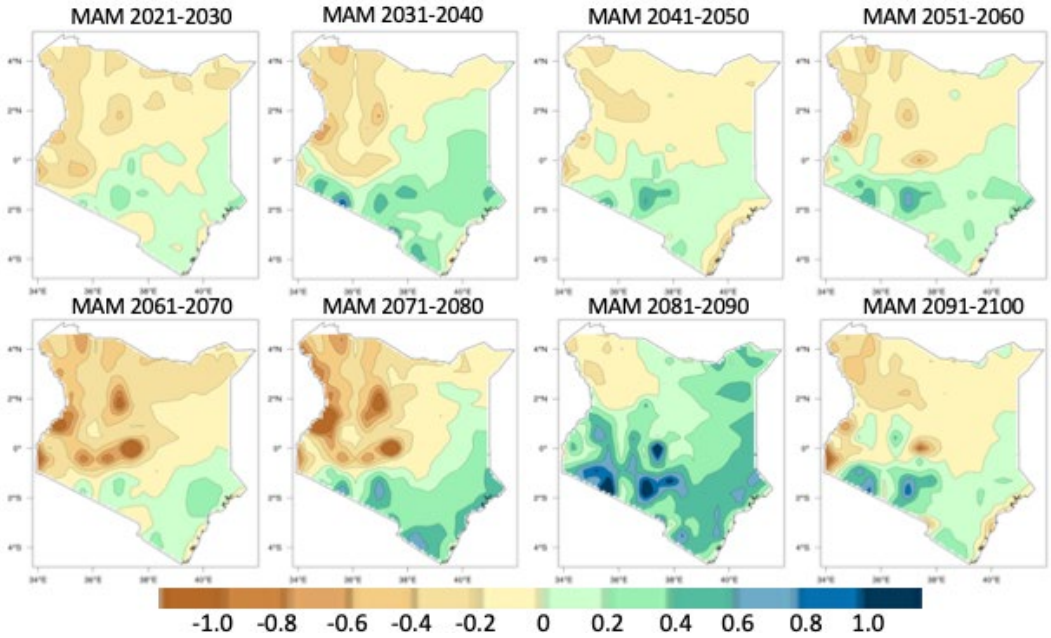

Figure 34: March-May seasonal rainfall changes (mm/day) over Kenya obtained from ensemble means of four top performing RCMs under the RCP8.5 scenarios for future ten-year periods from 2021 relative to historical simulations for the period 1961–2000.

The projected OND seasonal rainfall changes are shown in Figures 35 and 36. The projected decadal OND seasonal rainfall changes (mm/day) over Kenya based on the ensemble means of the best four model runs under RCP 4.5 and RCP 8.5 scenarios. Although there are spatial variability over the 8 future decades, there is generally an increase in projected seasonal rainfall over Kenya for both RCP4.5 (Fig. 26) and RCP 8.5 (Fig. 27) scenarios compared to the 1960-2000 present climate simulations of best-model ensemble mean. The OND 2081-2090 decadal rainfall change shows the highest increase in future rainfall under the RCP 8.5 scenario.

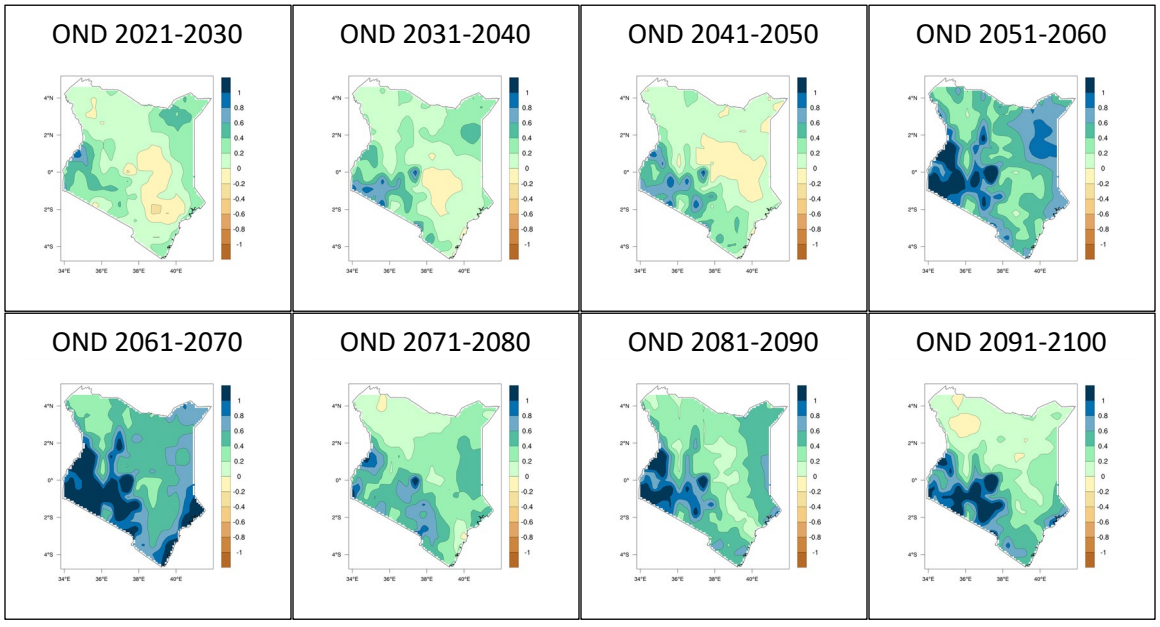

Figure 35: October-December seasonal rainfall changes (mm/day) over Kenya obtained from ensemble means of four top performing RCMs under the RCP4.5 scenario for future ten-year periods from 2021 relative to historical simulations for the period 1961–2000.

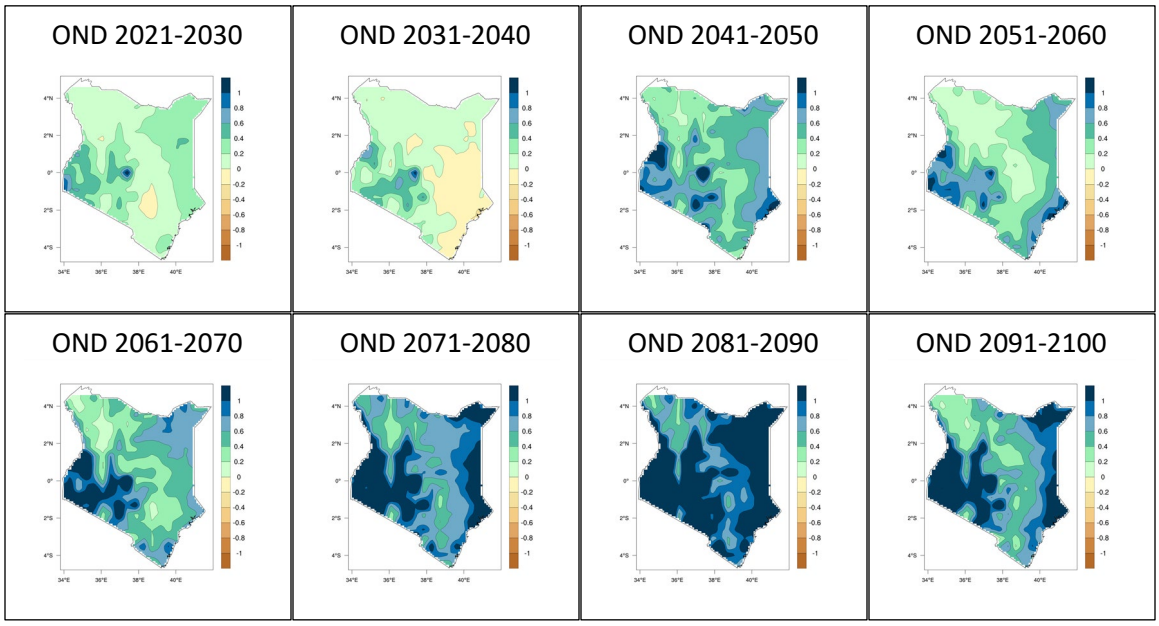

Figure 36: October-December seasonal rainfall changes (mm/day) over Kenya obtained from ensemble means of four top performing RCMs under the RCP8.5 scenarios for future ten-year periods from 2021 relative to historical simulations for the period 1961–2000.

In addition to spatial seasonal rainfall projected changes discussed above, the degree of dryness and wetness of rainfall changes are examined using 12-month Standardized Precipitation Index (SPI; WMO 2012) analysis for individual 30-year present climate (1976-2005) and three future climate periods (near-, mid- and far-future climates) under RCP4.5 and RCP8.5 scenarios. The SPI index is constructed by fitting a probability distribution to a long record of precipitation and transforming it to a normal distribution with zero mean. A 12-month SPI reflects long-term precipitation patterns. Distinctive wet and dry signals in 12-month SPI usually are tied with streamflows, reservoir levels, and even groundwater level at longer time scales (WMO 2012). According to WMO (2012), SPI values between -1.5 to -1.99 indicate “severe” dryness (wetness) while values less than -2.0 (greater than 2.0) indicate “extremely” dry (wet) climate. It is indicated further that a drought event occurs any time when the SPI is continuously negative and reaches an intensity of -1.0 or less.

The degree of dryness or wetness over Kenya is assessed using the “severe” and “extreme” categories and changes in projected SPI and frequency of dryness and wetness are examined for mid- and far-future climates under the RCP4.5 and RCP8.5 scenarios. Figure 28 provides the SPI over Kenya for different present and future periods and scenarios. Nationally averaged SPIs provide informative summary of precipitation differences between epochs and scenarios. SPI differences between the two scenarios in the present climate analysis are due to differences in the number of models used (three for RCP 4.5 and 4 for RCP 8.5). In addition to the response of climate to scenario forcing, temporal SPI variations for any epochs/periods depict the interannual variability of

rainfall across Kenya. Overall, longer and/or more frequent drier events are projected in the far-future climate under the RCP 8.5 scenario.

To further examine the spatial variations of severe to extreme dryness/wetness, analysis of the frequency of extreme dryness/wetness was conducted at individual grid points for different scenarios and periods relative to the 1976-2005 climate baseline. Accordingly, the percent of times that a given indicator exceeds a threshold for a given dryness/wetness is calculated for the present and projected climates and scenarios. Differences in frequency of occurrences between projected and present climates (future minus present) are used to assess future changes in severe/extreme dryness/wetness.

Figure 37 shows projected severe dryness (SPI between -1.5 to -1.99) changes for mid to far future periods relative to the present climate (1976-2005) under the RCP4.5 and RCP8.5 scenarios. For the present baseline climate, the percentage of severe droughts is higher for 4-model ensemble mean (RCP8.5) compared to the 3-model average for RCP4.5, especially in the Upper Athi river basin (Fig. 29 bottom-right). Although spatially mixed signals are indicated, severely dry climate is projected to intensify in the far-future period under the RCP 8.5 scenario. On the other hand, severely dry signals are projected to intensify in the mid-future period under the RCP4.5 scenario.

	RCP 4.5	RCP 8.5
Mid-future (2041-2070)	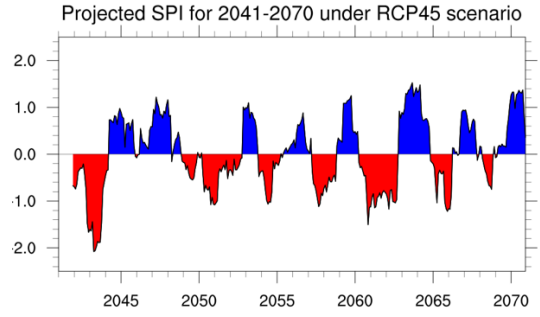	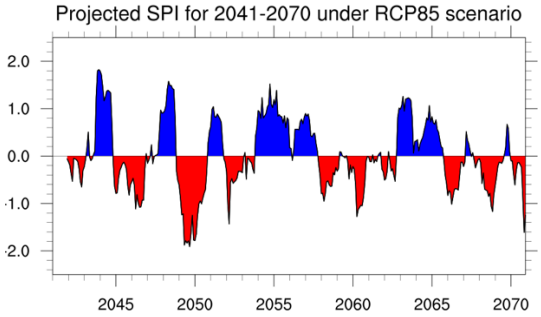
Far-future (2071-2100)	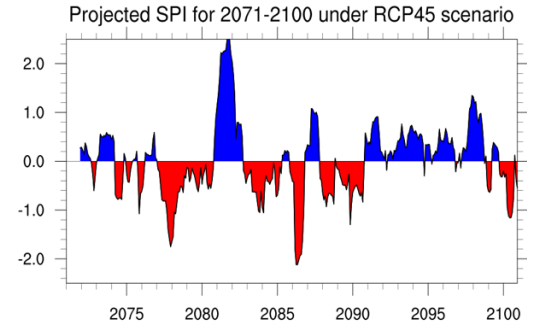	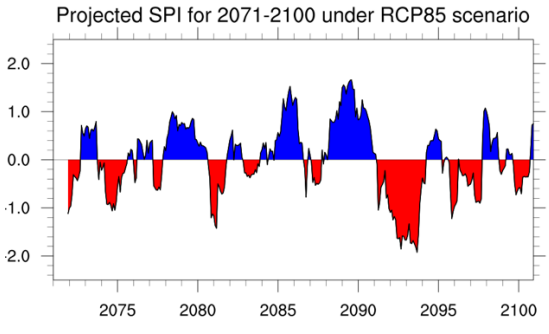

Present Climate (1976-2005)	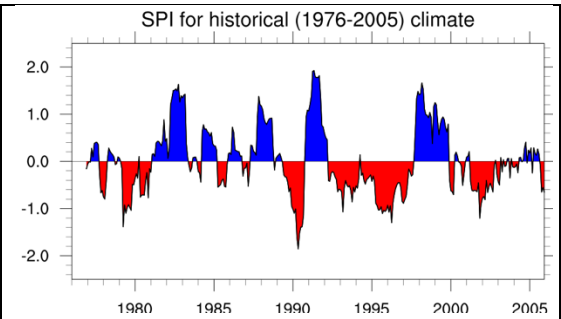	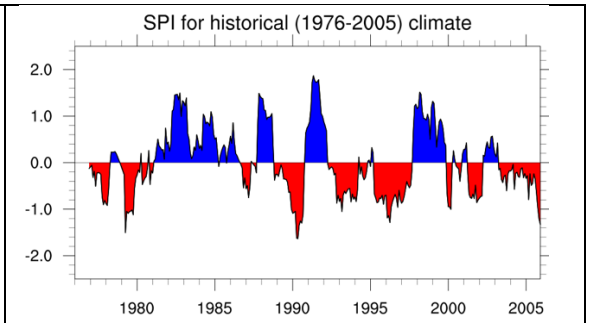
Present Climate (1961-2000)	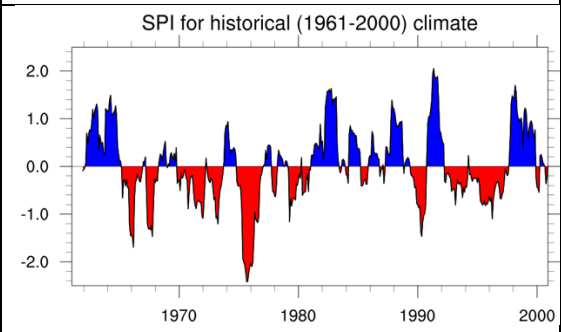	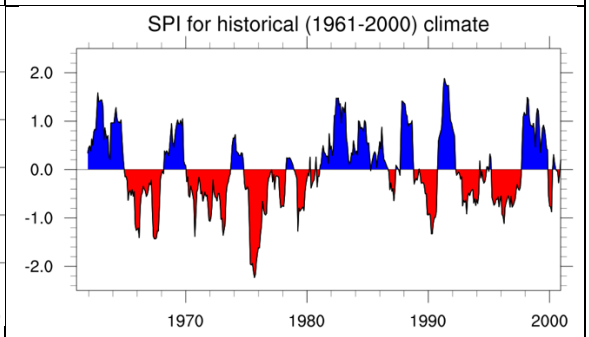

Figure 37: Twelve-month Standardized Precipitation Index (SPI) over Kenya for mid (2041-2070) and far(2071-2100) future climate periods under RCP4.5 (left) and RCP8.5 (right) scenarios. SPIs for two present climate periods (1975-2005 and 1961-2000; bottom two rows) are also provided under RCP4.5 (left) and RCP8.5 (right) scenarios. SPI differences in present climate between the two scenarios are due to differences in the number of models used (three for RCP 4.5 and 4 for RCP 8.5).

Figure 38 shows projected severe dryness (SPI between -1.5 to -1.99) changes for mid to far future periods relative to the present climate (1976-2005) under the RCP4.5 and RCP8.5 scenarios. For the present baseline climate, the percentage of severe droughts is higher for 4-model ensemble mean (RCP8.5) compared to the 3-model average for RCP4.5, especially in the Upper Athi river basin (Fig. 38 bottom-right). Although spatially mixed signals are indicated, severely dry climate is projected to intensify in the far-future period under the RCP 8.5 scenario. On the other hand, severely dry signals are projected to intensify in the mid-future period under the RCP4.5 scenario.

	RCP 4.5	RCP 8.5	
Projected changes in severe dryness/droughts in the mid-future (2041-2070) relative to current climate (2076-2005)	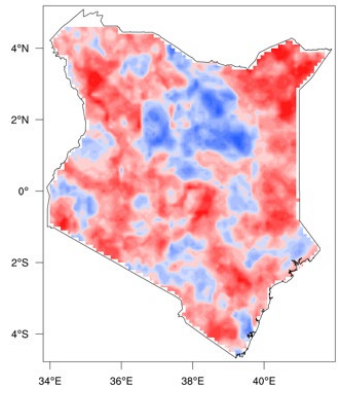	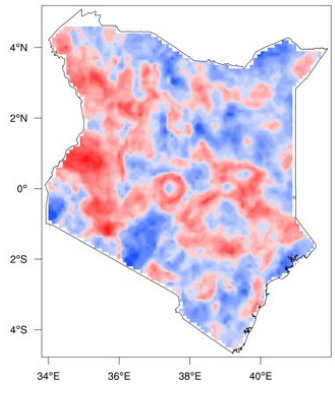	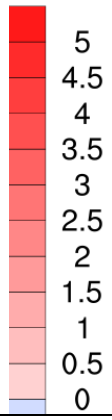

Projected changes in sever dryness/droughts in the far-future (2071-2100) relative to current climate (2076-2005)	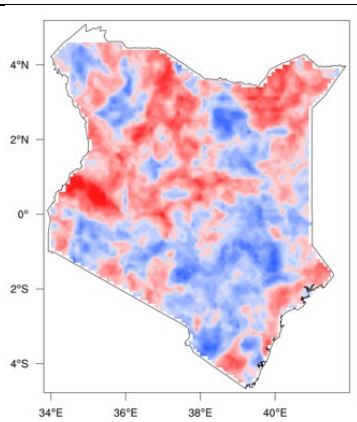	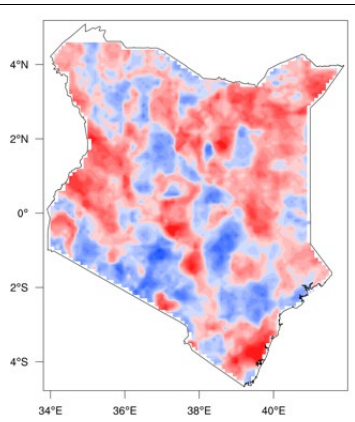	
Frequency (%) of severe dryness/droughts for the present climate (1976-2005)	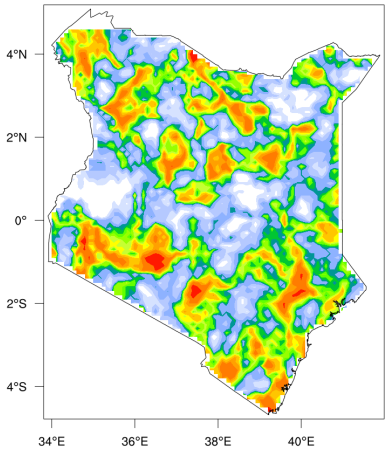	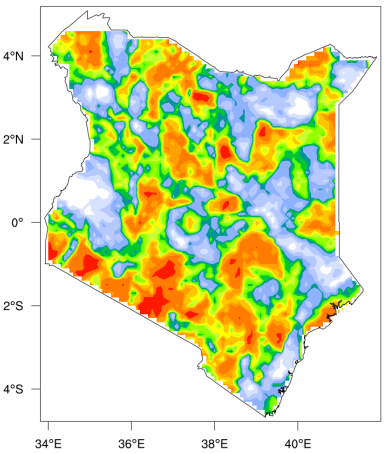	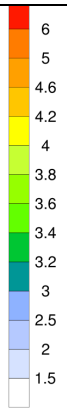

Figure 38: Projected changes in severe dryness/droughts for mid (1941-2070; top) and far (2070-2100; middle) future periods relative to the current (1976-2005) climate baseline (bottom row) under RCP 4.5 (left) and RCP 8.5 (right) scenarios.

	RCP 4.5	RCP 8.5	
Projected changes in extreme dryness/droughts in the mid-future (2041-2070) relative to current climate (2076-2005)	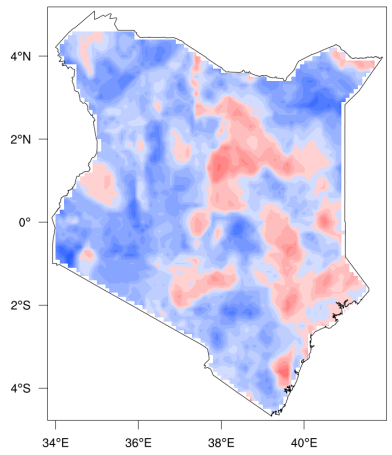	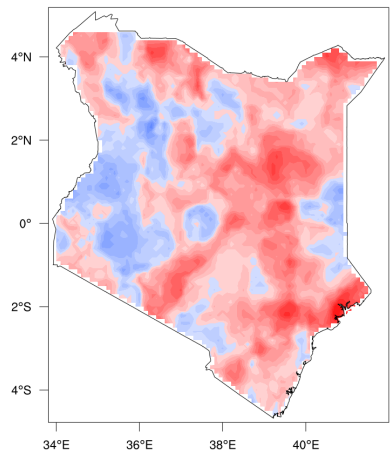	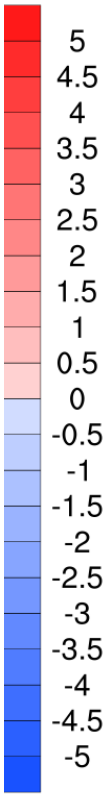
Projected changes in extreme dryness/droughts in the far-future (2071-2100) relative to current climate (2076-2005)	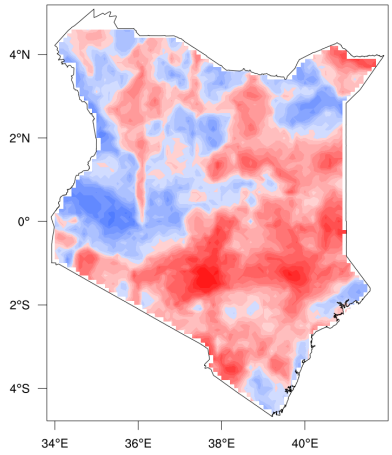	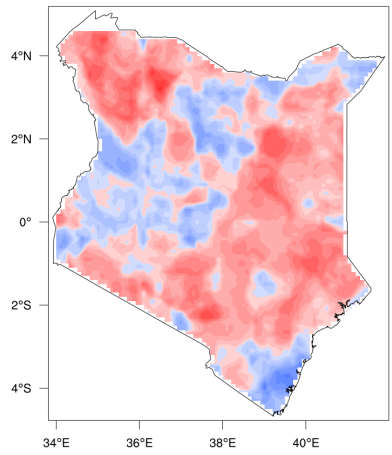	
Frequency (%) of extreme dryness/droughts for present climate (1976-2005)	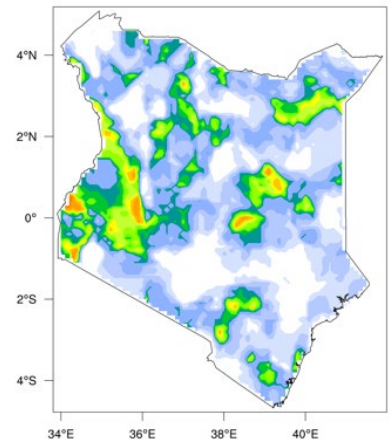	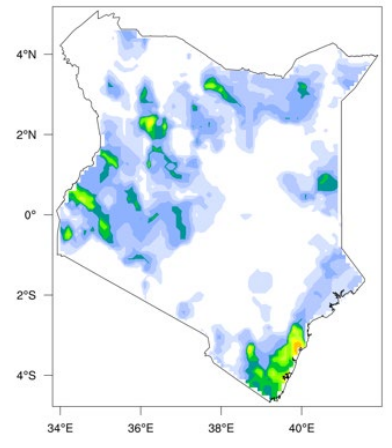	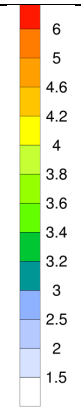

Figure 39: Projected changes in extreme dryness/droughts for mid (1941-2070; top) and far (2070-2100; middle) future periods relative to the current (1976-2005) climate baseline (bottom row) under RCP 4.5 (left) and RCP 8.5 (right) scenarios.

Although the frequencies of extreme drought (SPI less than -2.0) occurrences in the baseline climate are much lower than the baseline values for severe drought events, projected changes in extreme droughts have spatially more consistent and widespread signals under both RCP 4.5 and RCP 8.5 scenarios (Fig 39). Accordingly, extreme droughts are projected to increase from mid- to far-future periods under the RCP 8.5 scenario across much of the Upper Athi river basin. Increase in extreme drought occurrences are also projected in the far-future period under the RCP 4.5 scenario. It is to be noted that the baseline frequency values for extreme dryness are low because of the rarity of events with such high threshold value. However, the projected changes are substantially higher for the extreme drought indicator than severe drought case when both are refereed to their respective baseline climates.

Figure 39 shows projected severe wetness (SPI between 1.5 and 1.99) changes for mid to far future periods relative to the present climate (1976-2005) under the RCP4.5 and RCP8.5 scenarios. For the present baseline climate, the percentage of severe wetness is higher for 4-model ensemble mean (RCP8.5) compared to the 3-model average for RCP4.5, especially in the Upper Athi river basin (Fig. 40 bottom-right). Although spatially mixed signals are indicated, severely wet climate is projected to intensify in the far-future period under the RCP 8.5 scenario. On the other hand, severely wet signals are projected to intensify in the mid-future period under the RCP4.5 scenario.

	RCP 4.5	RCP 8.5	
Projected changes in severe wetness in the mid-future (2041-2070) relative to current climate (2076-2005)	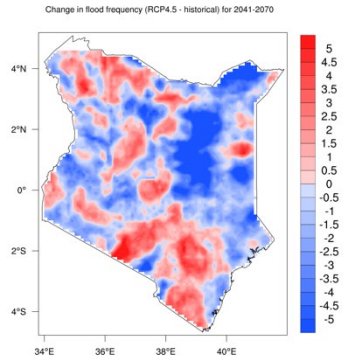	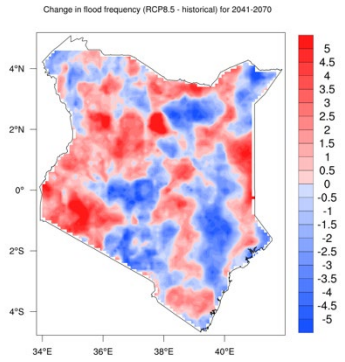	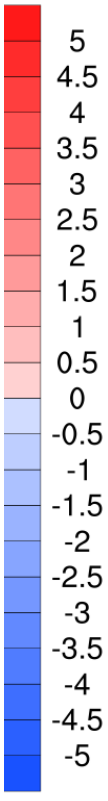
Projected change in severe wetness in the far-future (2071-2100) relative to current climate (2076-2005)	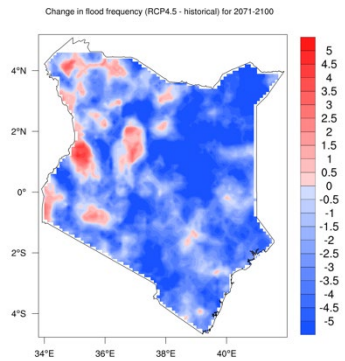	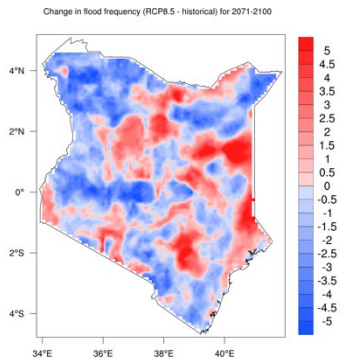	

Frequency (%) of severe dryness/droughts for present climate (1976-2005)	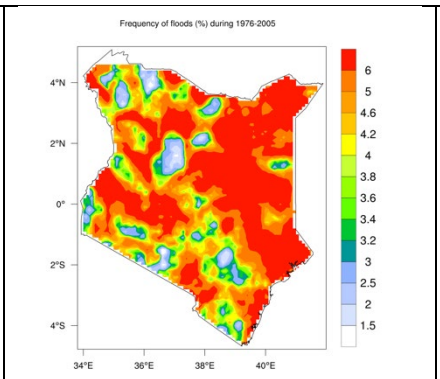	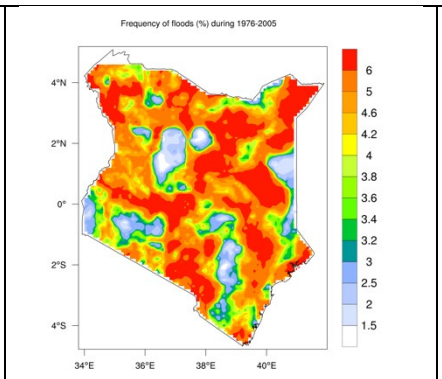	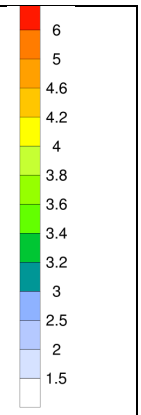

Figure 40: Projected changes in severe wetness for mid (1941-2070; top) and far (2070-2100; middle) future periods relative to the current (1976-2005) climate baseline (bottom row) under RCP 4.5 (left) and RCP 8.5 (right) scenarios.

	RCP 4.5	RCP 8.5	
Projected changes in extreme wetness in the mid-future (2041-2070) relative to current climate (2076-2005)	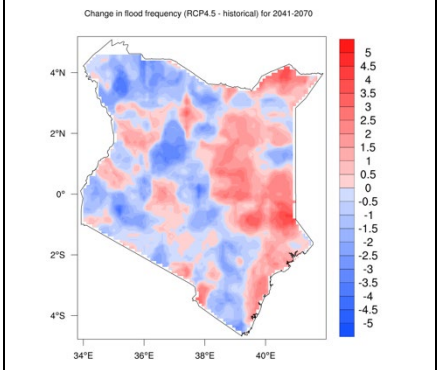	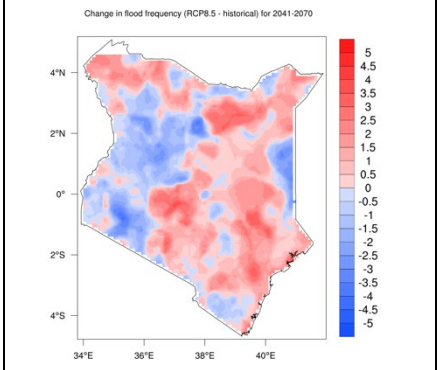	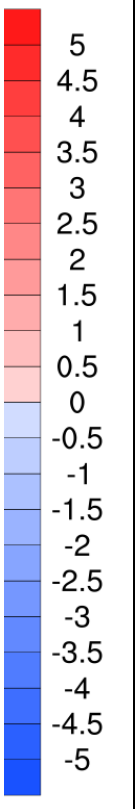
Projected change in extreme wetness in the far-future (2071-2100) relative to current climate (2076-2005)	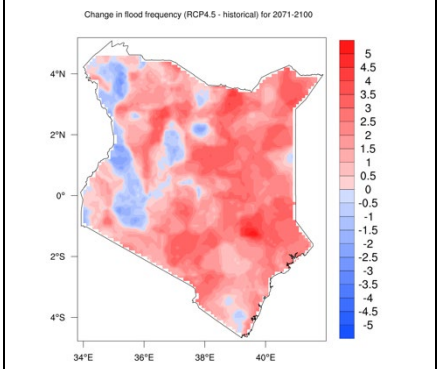	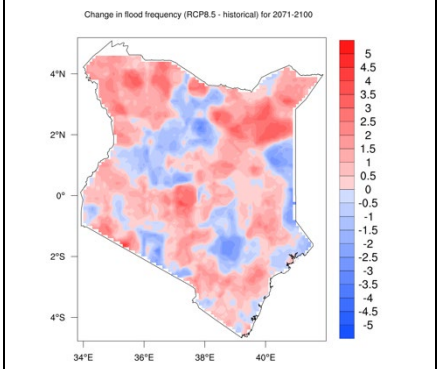	

Frequency (%) of extreme dryness/droughts for present climate (1976-2005)	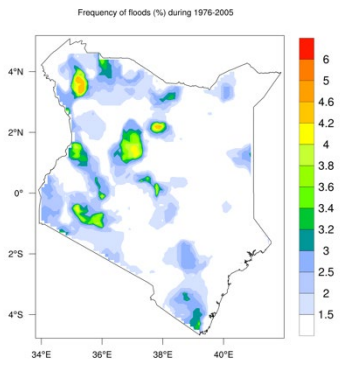	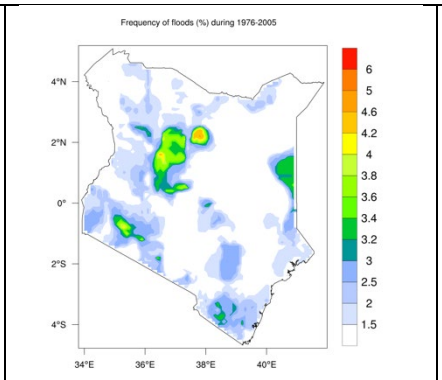	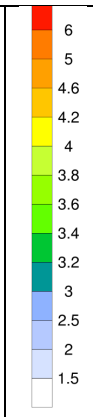

Figure 41: Projected changes in extreme wetness for mid (1941-2070; top) and far (2070-2100; middle) future periods relative to the current (1976-2005) climate baseline (bottom row) under RCP 4.5 (left) and RCP 8.5 (right) scenarios.

Although the frequencies of extreme wetness (SPI greater than 2.0) occurrences in the baseline climate are much lower than the baseline values for severe wet events, projected changes in extreme wetness have spatially more consistent and widespread signals under both RCP 4.5 and RCP 8.5 scenarios (Fig 32). Accordingly, extreme wetness are projected to increase from mid- to far-future periods under the RCP 8.5 scenario across much of the Upper Athi river basin. Increase in extreme wetness occurrences are also projected in the far-future period under the RCP 4.5 scenario. It is to be noted that the baseline frequency values for extreme wetness are low because of the rarity of events with such high threshold value. However, the projected changes are substantially higher for the extreme wetness indicator than severe wetness case when both are refereed to their respective baseline climates.

5.0 Conclusion

In terms of trend, MAM rainfall has been on the decline with the recent decade 2000-2010 recording a depressed rainfall compared to the other decades. While that of OND showed an increasing trend. Although there is an increase and decrease in OND and MAM seasonal rainfall respectively, however, some stations showed an opposite trend. Maximum and minimum temperature had an increasing trend, with an average increase of 0.3 to 1.44 oC, the increase was more during the cold months than the other months. The skill of the regional models in simulating rainfall was good for half of the models and poor for the other half, especially for the northeastern part of the study area. The model captured the spatial and temporal variability of rainfall over Kenya; however, over-estimation and under-estimation were noted in some parts of the study area.

All the models did not capture the seasonal peaks of April and November for MAM and OND respectively. All models were skillful in simulating minimum and maximum temperature than that of rainfall. They captured well the annual cycle and spatial variability of both minimum and maximum temperature over Kenya. The regional models were also skillful in reproducing the effects of large-scale circulation signal on Kenya rainfall. Different models projected rainfall differently, with some indicating Kenya is becoming wetter over time while

others indicating drier condition expected. On a seasonal scale, MAM is projected to decrease over most part of the study area, while that of OND is expected to increase this is under RCP8.5 emission scenario. Under RCP4.5, both seasons are expected to decrease.

Therefore, higher emissions are likely to benefit Kenya with an increase in OND rains than average emission. Temperature will become hotter under both scenarios RCP4.5 and RCP8.5 emission, with an average increase of 0.3 to 5 0C at the end of 21st century. An increasing trend in warm extreme and decrease in cold extremes is likely, warm days and nights also showed an upward trend. On the contrary, precipitation patterns had mixed results with HIRHAM showing increasing trends in most of precipitation extreme indices, while the other models showed a decreasing trend. Under both scenarios considered in this study, variability of rainfall extremes is expected to be high compared to the shift to higher or low climate extremes. Uncertainties still remain in the future changes in precipitation, different models projected differently for rainfall over the study area but there was better agreement in temperature projection

The study established that MAM rainfall has been on the decline and is projected to decrease, while that OND is projected to increase. The changes are not uniform from one region to another. Future changes that are expected to occur are different from one climatological zone to another. Future rainfall variability is also expected to increase, therefore climate extremes of drought and floods are expected to increase its frequency and intensity toward the end of 21st Century. And these will result in economic losses to communities because of over dependency on rained agriculture. Temperature is also anticipated to increase, which cause might cause frequent heat wave especially in the low lying areas and also increase evapotranspiration and thus affecting agriculture. Crop production and livestock keeping will be greatly negatively impacted by decrease in the rangeland for livestock keeping these will lead to lose of livelihood for many households and will lead to over reliance on government relief food and increase conflict over resources. It was established high heat stress will increase heat related health risks more especially to the vulnerable. Due to projected increase in temperature and the rapid expansion of urban areas, urban heat island will affect the urban dweller, where night time temperature will generally increase.